Chapter 5

A Study on Structure and Dynamics of wild type DNA/DNA, RNA/DNA and RNA/RNA hybrid duplexes in complex with Human RNase H catalytic domain.

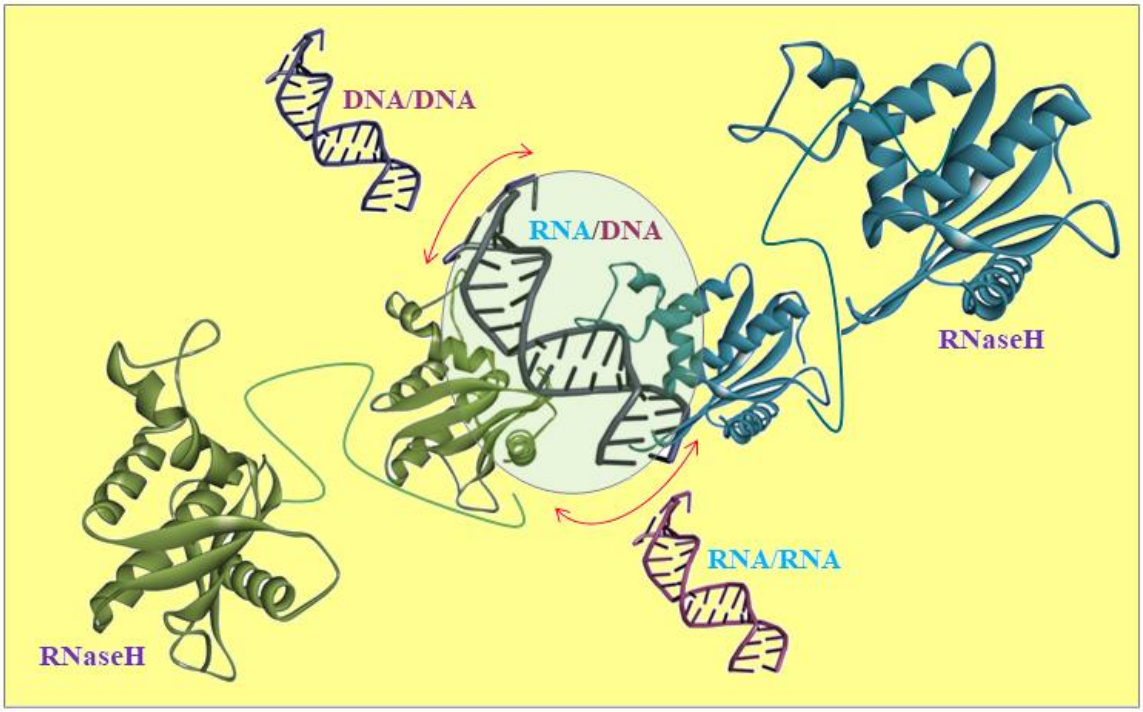

5.1. Introduction

A majority of diseases in people are caused by abnormal protein synthesis or abnormal protein activity. These disease-causing proteins can be stopped by preventing the transfer of genetic information from DNA to mRNA which can be achieved by antisense oligonucleotide-based medications (ASOs/AONs) that complementary bind a nucleic acid sequence to specific mRNAs employing *Watson-Crick* base pair hybridization [1-2]. In contrast to the use of conventional medicines, usage of ASOs as medicinal agents constitutes a unique therapeutic method [3-4]. Unlike monoclonal antibodies and pharmaceutical substances these synthetic ASOs/AONs bind with their corresponding sense mRNAs and limit the production of disease-causing proteins, which is the anticipated therapeutic effect. ASOs can be created to treat a variety of gene-transmitted diseases, such as cancer, cardiovascular conditions, as well as numerous inflammatory and infectious diseases [5-9]. These antisense-driven treatments have higher specificity, making them more potent and beneficial over conventional drugs.

Antisense oligonucleotides (ASOs) are modified nucleic acids that have been chemically altered to achieve complementarity with their target mRNAs [10]. These ASOs/AONs form hybrid duplexes with the target mRNAs through *Watson-Crick* base pairing. Depending on the oligonucleotide chemistry, there are a number of ways for antisense-mediated gene inactivation. The two most frequent are translation arrest caused by steric obstruction of ribosomal read-through and enzymatic cleavage of the mRNA strand by recruitment of Cellular Endonuclease Ribonuclease H (or RNase H) [11-13]. In the RNase H dependent mechanism of antisense activity, an ASO binds to an mRNA, activates the RNase H which selectively cleaves the mRNA strand from the ASO/mRNA hybrid duplexes [14-16].

The RNA strand of DNA/RNA duplexes is the common substrate specificity for the RNase H family of non-sequence-specific endonuclease enzymes [17-18]. By breaking phosphodiester bonds in the RNA backbone to leave behind a 3' hydroxyl and a 5' phosphate group, the RNase H hydrolyses the cleavage of RNA in a DNA/RNA substrate. The conserved sequence motif, known as the DEDD motif, is the focal point of the active site of all RNases H. It is made up of four negatively charged amino acid residues: aspartate, glutamate, and a histidine residue. These charged residues are by definition directly involved in the catalytic function and require two metal ions for

catalysis. Under physiological conditions, a two-metal-ion catalysis mechanism involving magnesium and manganese ions cleaves the phosphodiester bonds of RNA on either end of the cut site [19]. Experimental and computational data indicate that the enzyme activates a water molecule bonded to one of the metal ions via the conserved histidine. An intermediate is created when the transition state combines with the protonated phosphate and the deprotonated alkoxide leaving group. The leaving group is protonated by glutamate, which has a higher pKa. Nevertheless, it is still unknown, how the cleft product releases itself. Experimental evidence from time-resolved crystallography and related nucleases indicates that a third ion is brought into the process's active site.

In chapter 3 we studied the structural and electronic properties of some existing antisense modifications (ASOs) both at the monomer and at the oligomer level. Due to their inherent instability in biological environments, ASOs tend to degrade rapidly even before forming duplexes. To address this issue and ensure a robust antisense response, chemical modifications are required to enhance their stability, binding affinity, and facilitate cellular uptake. The concept of using ASOs as therapeutic agents was first introduced by Zamecnik and Stephenson in 1978 [20] and up till date phosphorothioates are known to best serve as substrates for RNase H when bound to their complementary RNA targets however with slightly lower *activity* than the natural phosphodiester oligonucleotides [21-26]. Thus, in chapter 4, we tried to propose a few novel antisense modifications which may be useful to pharma industries, and studied their structural and electronic properties both at the monomer and at the oligomer level. However, for successful clinical application, the modified ASOs should possess high resistance to endonucleases RNase H, high affinity for target complementary RNA sequences and bind by *Watson-Crick* base pairing forming ASO/RNA duplexes along with excellent RNA selectivity. The cellular endonuclease RNase H is activated by the ASO/RNA duplexes which specifically cleaves the RNA strand from the ASO/RNA duplexes in a targeted manner. With the gapmer method, oligonucleotides with increased affinity for RNA targets and coupled RNase H activity can be produced. Additionally, chimeric oligonucleotides with modified wings and with gaps more than five deoxynucleotides in the gap show effective antisense activity [27-31]. Gaps of less than four deoxynucleotides do not allow RNase H to cleave of the target RNA and those with gaps of five deoxynucleotides are cleaved at 3-fold slower rate than unmodified substrates.

Cleavage of the duplexes by RNase H is the most desirable antisense mechanism. Thus, when the RNA substrate is organized, the rate of RNase H cleavage is greatly decreased. To elucidate the structural and functional significance of RNase H, a thorough investigation employing the RNase H is required to know the mechanism of interaction of the RNase H with the wild type duplexes as DNA/DNA, RNA/RNA homo duplexes and DNA/RNA hybrid duplexes. Henceforth, the present chapter aims to identify the important amino acid residues which might play an important role in stabilizing wild type duplexes at the active site of RNase H and in molecular recognition of the RNase H in specifically identifying the RNA strand from the wild type duplexes. Accordingly in the subsequent chapter 6, we will study the structure and dynamics of the various ASO/RNA hybrid gapmer-type duplexes of both existing and the proposed novel antisense modifications in complex with RNase H catalytic domain.

By reducing the ASO length (from 20-mer to 14-mer), the potency of MOE based ASOs in animals was increased 3- to 5-fold ($ED_{50} \approx$ 2-5 mg/kg) without producing hepatotoxicity. But results from chapter 3 and 4 elucidated that the 14-mer duplexes were too small to be stable and to study elaborate structural and dynamics at a scale of 1 μs simulation time. Longer duplexes can provide a larger sample size, which will increase the statistical power of the study and that any observed effects or behavior are more likely to be meaningful and not just random fluctuations. Thus, studying long duplexes (long DNA or RNA strands) over small duplexes can provide more comprehensive insights into the behavior and properties of nucleic acids. In biological systems, nucleic acids often exist as long strands rather than short segments. By studying long duplexes, we can better mimic the natural conditions and interactions of nucleic acids, understand more of complex interactions, such as secondary structures, tertiary interactions, and cooperative binding effects. Longer duplexes also enable the identification and characterization of sequence motifs and structural elements that may not be present or easily discernible in shorter duplexes. These motifs can be important for regulatory functions or for interactions with other molecules. While studying small duplexes can be valuable for understanding specific aspects of nucleic acid structure and function, studying long duplexes offers a more comprehensive view that better reflects biological reality and has broader applicability. Thus, the goal of the subsequent chapters is to evaluate the structure-activity relationship of 20-mer duplexes complexed with a Human RNase H catalytic domain.

5.2. Materials and Methods

5.2.1. Systems building for MD simulations

This chapter describes the structure and dynamics of wild type DNA/DNA, RNA/DNA and RNA/RNA duplexes in complex with a Human RNase H catalytic domain. Starting structures of the duplexes were built on the crystal structure of a 20-mer RNA/DNA substrate complexed with Human RNase H1 catalytic domain (PDB ID: 2QKB as reported by *Nowotny et al.*) [32]. The built in duplexes include the wild type DNA/DNA, RNA/DNA and RNA/RNA duplexes. The AMBER software programs all-atom MD simulation framework was used for building of the duplexes and running the MD simulations [33]. Gaussian09 software was used to derive partial atomic charges at the M06-2X/-311G** level of theory and RESP fitting was completed using the antechamber module of AMBER [34-35]. Five residues from ASO strand's 5′ and 3′ end was specifically modified integrating them into gapmer-type duplexes. The systems were explicitly solvated with TIP3P water boxes after the charge was neutralized by the addition of Na^+/Cl^- as counter ions [36]. Using the leap module, the complete duplex building process was carried out implementing the standard force field parameters "DNA.OL15" for DNA and "RNA.OL3" for RNA [37-38].

5.2.2. Simulation Protocol and Trajectories Analyses

The built-in systems were energy minimized to create correct initial structures wherein initial positional restrictions of 100 kcal/mol were used to keep the solute atoms stable, which was then followed by a gradual reduction and eventual removal of all restrictions. Energies were minimized using the steepest descent method for 5000 steps. The systems were then heated gradually from 0 K to 300 K in NVT canonical ensemble with 100 kcal/mol limitations on each solute atom. Following heating, the systems proceeded through equilibration with initial restrictions of 100 kcal/mol and gradually relaxing the constraints on every solute atom in NPT conditions. The systems were then allowed to simulate under production run conditions for 1 μs simulation time and the trajectories were used for analysis. Particle Mesh Ewald approach was used to simulate the system under periodic boundary conditions while taking the long-range electrostatics into consideration [39]. The SHAKE method was used to perform MD integration with a 2.0 fs time step on all bonds containing hydrogen atoms [40]. Langevin temperature equilibration scheme was used to maintain the system temperature. The cut-off distance for non-bonding encounters has been set at 10. NPT conditions were maintained

throughout the production simulation run and the pair-list was updated at every 5000 steps. To account for the statistical variance in the computations, replica sets of MD simulations accounting to two data sets Set-I & Set-II were performed, each trajectory corresponding to 1 μs simulation time. The RMSD, RMSF, sugar pucker, N-glycosidic dihedral angles, inter-strand and intra-strand phosphate distances, H-bonds, Solvent Accessible Surface Area (SASA) all were computed using the CPPTRAJ module of Amber Tools [41]. Base-pairing, Base-stacking and Helix-turning all were observed using the NASTRUCT module of AMBER. The free energies of all the duplexes were calculated using the MMGBSA module of AMBER [42].

5.3. Results and Discussion

5.3.1. Stability of the DNA/DNA, RNA/DNA and RNA/RNA duplexes

Simulations were conducted considering wild type duplexes (a) DNA/DNA (b) RNA/DNA (c) RNA/RNA without RNase H and the wild type duplexes complexed with RNase H (d) DNA/DNA-RNaseH (e) RNA/DNA-RNaseH and (f) RNA/RNA-RNaseH. To understand how the duplexes structural characteristics changed over the course of simulation, structures of the duplexes have been pictured at 500th ns and 1000th ns from the 1 μs simulation trajectory, plotted in Figure 5.1, for both of the simulation sets (Set-I & Set-II). From Figure 5.1 it is observed of the bare duplexes to exhibit stable *Watson-Crick* base-pairing, base-stacking and helix-turning to be maintained throughout the simulation time. The duplexes complexed with RNase H were also stable at the catalytic domain of the RNase H maintaining stable *Watson-Crick* base-pairing, base-stacking pattern and helix-turning. The structures acquired from the complete simulation trajectory were compared with their respective initial structures reviewing the RMSD plots encompassing the whole duplex presented in Figure 5.3 and RMSD plots of the RNaseH alone are plotted in Figure 5.2. Each of the duplexes appeared to be fluctuating potentially within and around a range of 2 to 6 Å RMSD values. Calculated average RMSD values of the systems (a)-(f) exhibited an average RMSD of 4.34, 3.94, 3.79, 4.05, 3.41, 4.35 Å and 4.67, 3.47, 3.62, 4.90, 4.05, 4.81 Å for Set-I and Set-II, respectively. RMSD of (a) DNA/DNA and (d) DNA/DNA-RNaseH is higher for both the sets of simulation. The duplexes overall RMSD data over time indicated that duplex stability is well preserved in each case for the entire simulation trajectory for both the sets of simulation.

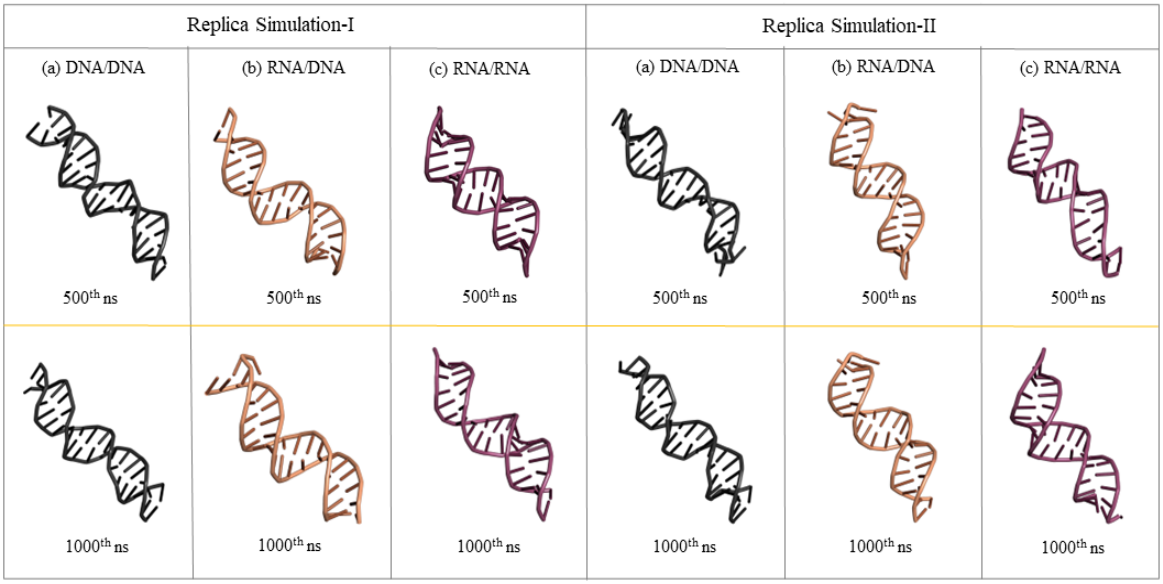

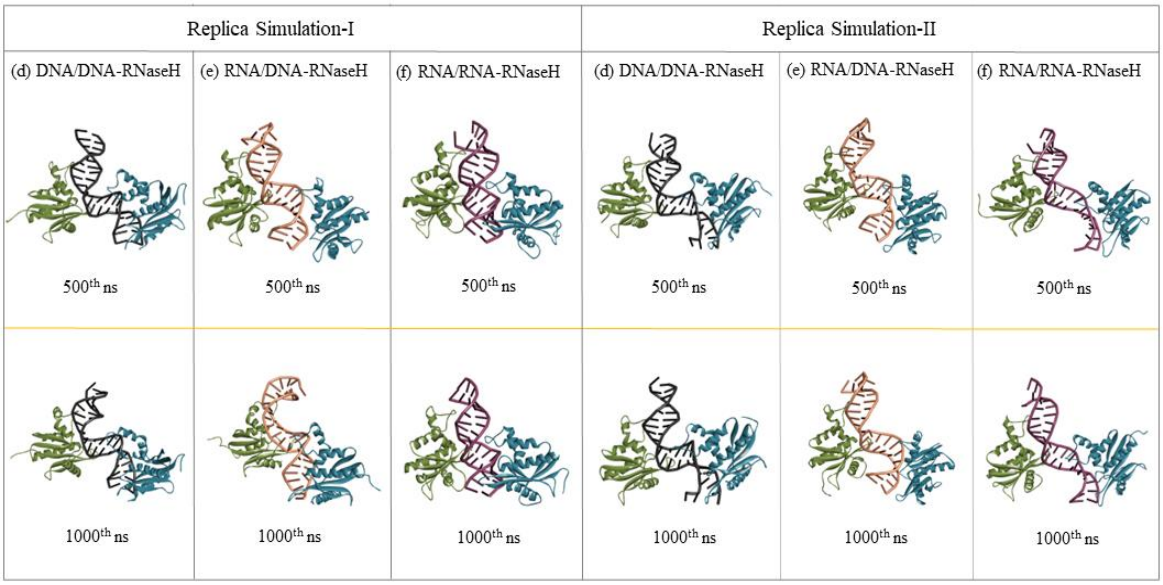

Figure 5.1: Structures of the wild type duplexes (a) DNA/DNA (b) RNA/DNA, (c) RNA/RNA and the wild type duplexes complexed with dimeric RNaseH (d) DNA/DNA-RNaseH (e) RNA/DNA-RNaseH and (f) RNA/RNA-RNaseH at 500th ns and end structures at 1000th ns obtained from the 1 µs simulation trajectory, for both the sets of simulation [Set-I & Set-II].

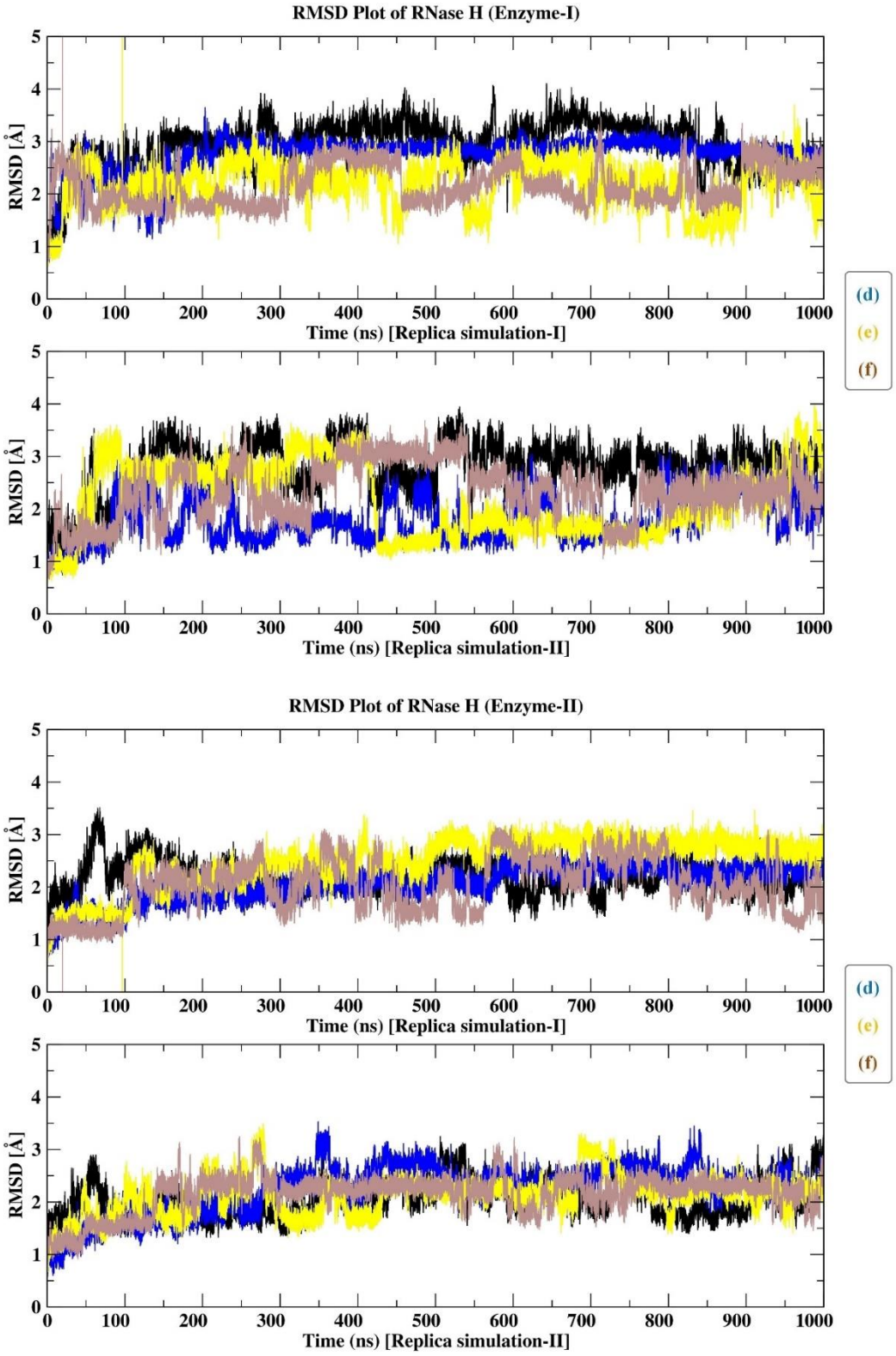

Figure 5.2: RMSD plots of the RNase H alone from the (d) DNA/DNA-RNaseH (e) RNA/DNA-RNaseH and (f) RNA/RNA-RNaseH complexes of simulation trajectories from two data sets [Set-I & Set-II] each simulated for 1 μs simulation time.

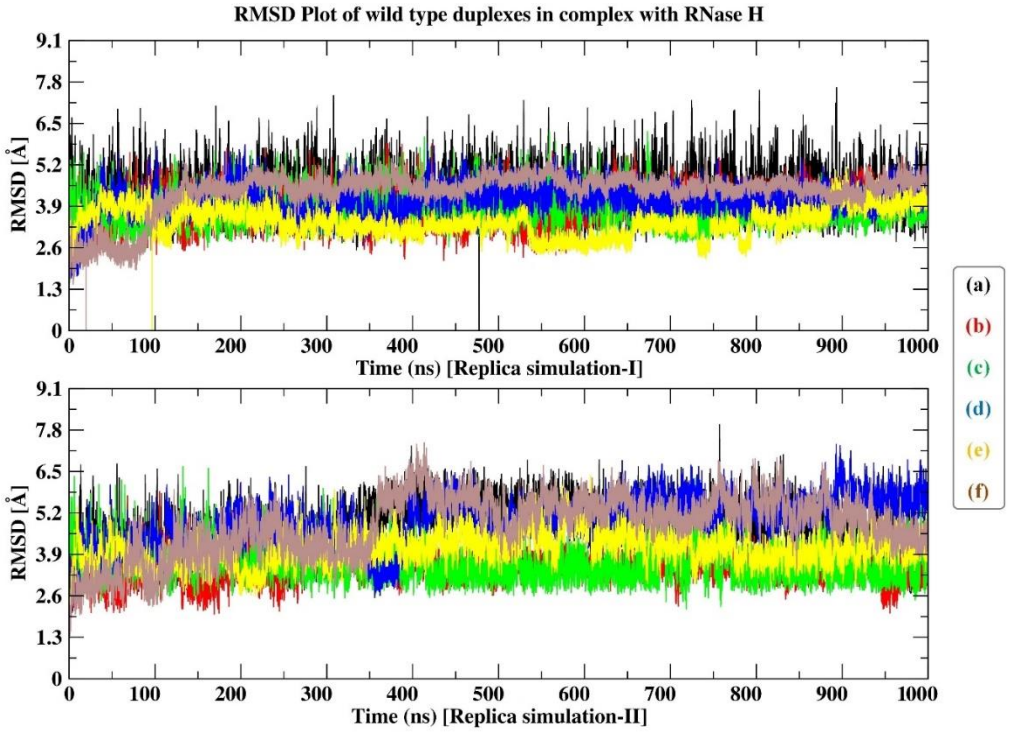

Figure 5.3: RMSD plots of (a) DNA/DNA (b) RNA/DNA, (c) RNA/RNA, (d) DNA/DNA-RNaseH (e) RNA/DNA-RNaseH and (f) RNA/RNA-RNaseH of simulation trajectories from two data sets [Set-I & Set-II] each simulated for 1 μs simulation time.

5.3.2. Oligomer Duplex Dynamic Structure: Inter-Strand and Intra-Strand PP distances of the DNA/DNA, RNA/DNA and RNA/RNA duplexes

Molecular double helix of nucleic acids is made up of two sugar-phosphate backbones twisted together to form the structural framework of duplexes. Longer intra-strand phosphate-phosphate (PP) distances (~7 Å) are used to explain the *C2'-endo* sugar puckering observed in *B-type* duplexes and shorter intra-PP distances (~5.9 Å) are used to describe the *C3'-endo* sugar puckering observed in *A-type* duplexes [43-44]. Average inter-PP and intra-PP distances of the wild type duplexes for both the strands for the entire simulation trajectory are plotted in Figure 5.4 and Figure 5.5 respectively. Inter-strand PP distances describe the overall width of the and in Figure 5.4, duplexes are seen to be lying in the acceptable range of 19-20 Å, for both the sets of simulations (Set-I & Set-II), for the entire simulation time.

In Figure 5.5, clear distinction is observed for the DNA, RNA residues where the DNA residues are exhibiting intra-strand PP distances greater than RNA residues, for homoduplexes. However, residues are seen to fluctuate more in case of the hybrid

duplexes. The increased fluctuation observed in RNA/DNA hybrid duplexes compared to DNA/DNA and RNA/RNA non-hybrid duplexes can be attributed to several factors:

Chemical Differences: DNA and RNA have different chemical properties due to variations in their sugar backbones (deoxyribose in DNA vs. ribose in RNA) and nucleobases (thymine in DNA vs. uracil in RNA). These chemical differences can lead to variations in the stability and dynamics of hybrid duplex formation, resulting in increased fluctuation.

Base Pairing Specificity: RNA/DNA hybrids may exhibit different base pairing specificities compared to DNA/DNA or RNA/RNA duplexes due to the presence of both RNA and DNA strands. The interactions between RNA and DNA bases may not be as stable or specific as those between two identical strands, leading to increased fluctuation in hybrid duplexes.

Structural Flexibility: RNA strands are generally more flexible than DNA strands due to the presence of an additional hydroxyl group in the ribose sugar. This increased flexibility can contribute to greater structural fluctuations in RNA/DNA hybrid duplexes compared to DNA/DNA and RNA/RNA duplexes.

Conformational Dynamics: The combination of RNA and DNA strands in hybrid duplexes can introduce additional conformational dynamics, such as fluctuations in backbone conformation and base stacking interactions. These dynamics may contribute to increased fluctuation in hybrid duplexes compared to homoduplexes formed by DNA/DNA or RNA/RNA interactions.

Protein Interactions: Hybrid duplexes may interact differently with proteins compared to homoduplexes formed by DNA/DNA or RNA/RNA interactions. Proteins involved in processes such as RNA processing, RNA interference, or DNA repair may recognize and bind specifically to RNA/DNA hybrids, leading to alterations in the stability and dynamics of these duplexes.

Overall, the combination of chemical differences, base pairing specificity, structural flexibility, conformational dynamics, and protein interactions may have contributed to the increased fluctuation observed in DNA/RNA hybrid duplexes compared to DNA/DNA and RNA/RNA hybrid duplexes.

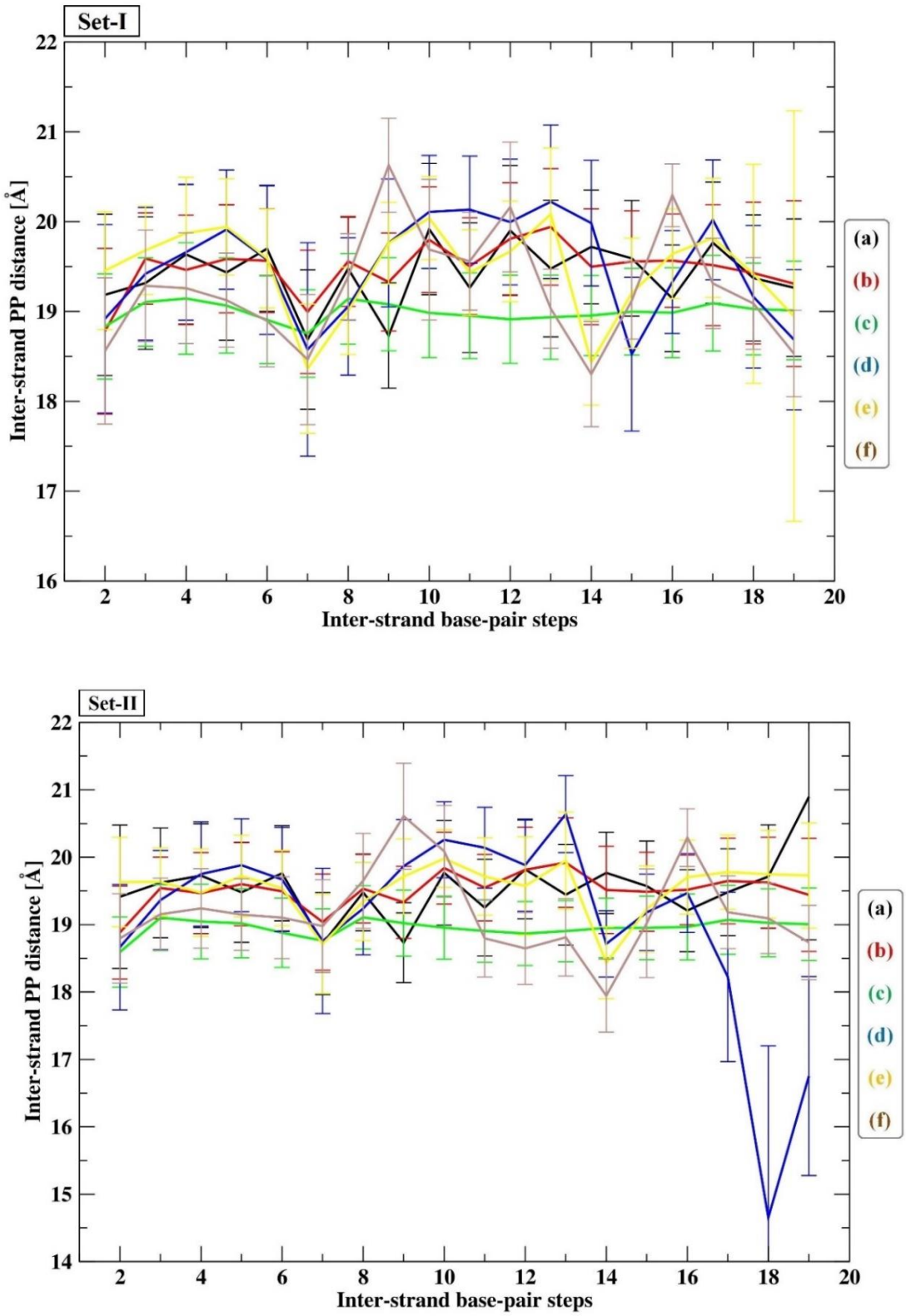

Figure 5.4: Inter-strand PP distance of (a) DNA/DNA (b) RNA/DNA, (c) RNA/RNA, (d) DNA/DNA-RNaseH (e) RNA/DNA-RNaseH and (f) RNA/RNA-RNaseH of simulation trajectories from two data sets [Set-I & Set-II] each simulated for 1 μs simulation time.

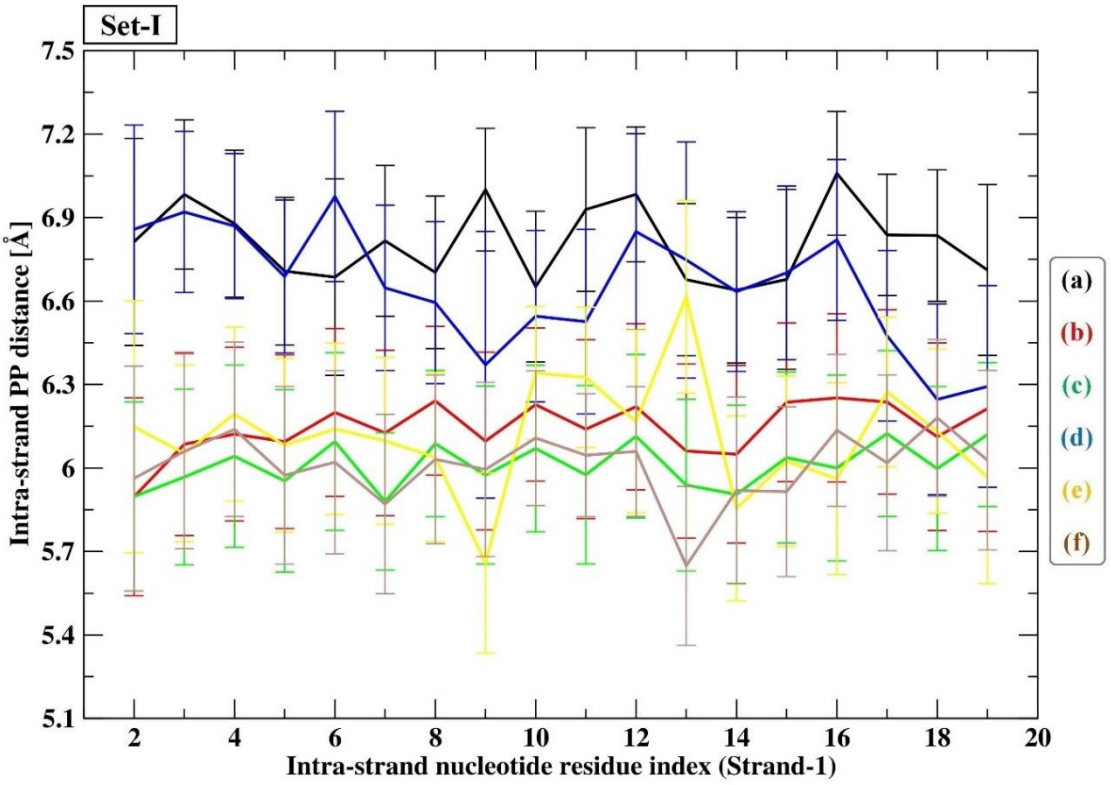
Set-I
Intra-strand PP distance [Å]
Intra-strand nucleotide residue index (Strand-1)
(a)
(b)
(c)
(d)
(e)
(f)

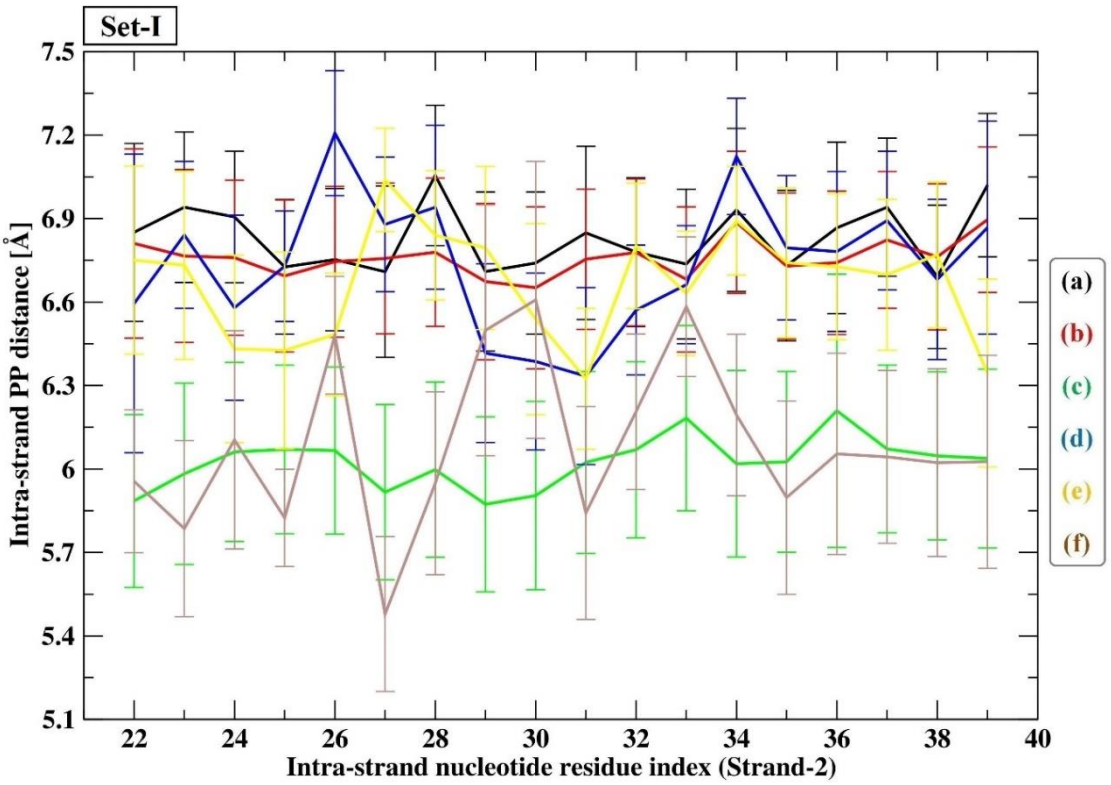
Set-I
Intra-strand PP distance [Å]
Intra-strand nucleotide residue index (Strand-2)
(a)
(b)
(c)
(d)
(e)
(f)

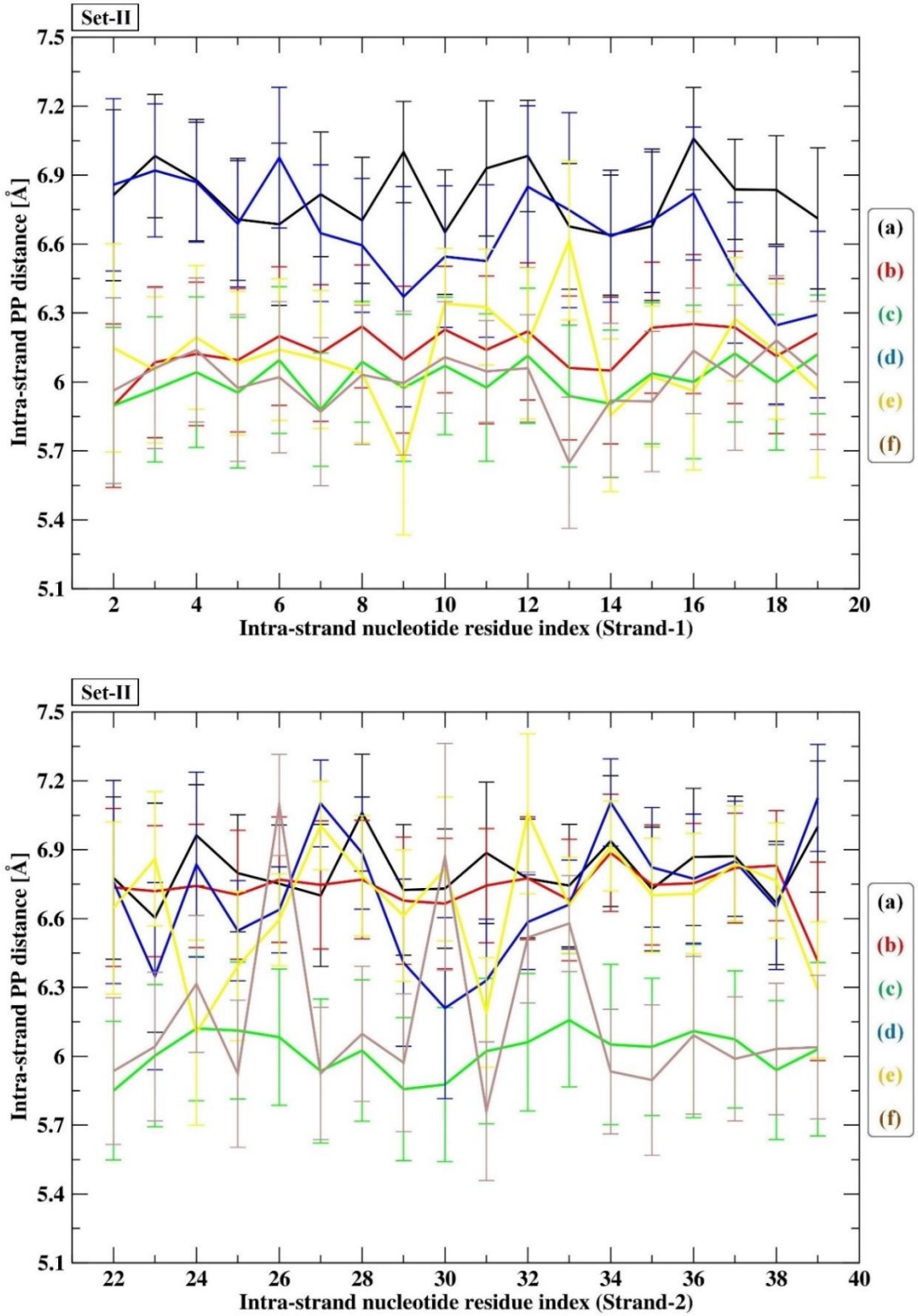

Figure 5.5: Intra-strand PP distance of (a) DNA/DNA (b) RNA/DNA, (c) RNA/RNA, (d) DNA/DNA-RNaseH (e) RNA/DNA-RNaseH and (f) RNA/RNA-RNaseH of simulation trajectories from two data sets [Set-I & Set-II] each simulated for 1 µs simulation time.

5.3.3. Torsion Angle Dynamics: Sugar-pucker and N-glycosidic torsion distribution of the DNA/DNA, RNA/DNA and RNA/RNA duplexes

The sugar-pucker conformation describes the orientation of the sugar ring with respect to the adjacent phosphate groups in the backbone of nucleic acids. The *A-form* and *B-form* conformations in a duplex, respectively, are represented by the sugar puckers in nucleic acids, which are either in the *C3'-endo* conformation (pucker phase values: 0°–40°) or the *C2'-endo* conformation (pucker phase values: 120°–180°) [45]. Bigger population of sugar puckers is directed by DNA into the *C2'-endo* conformation in an effort to produce an overall *B-form* geometry, and a larger population of sugar puckers is directed by RNA into the *C3'-endo* conformation in an effort to produce an overall *A-form* geometry. In DNA/DNA duplexes, the predominant sugar-pucker conformation is *C2'-endo,* and the glycosidic torsion angle tends to favor the anti-conformation. In RNA/DNA and RNA/RNA duplexes, the sugar-pucker conformation can include both *C2'-endo* and *C3'-endo*. Sugar pucker distribution of nucleotide residues throughout the duplexes are presented in Figure 5.6 to estimate the extent of such conformational integration of the sugar puckers. According to Figure 5.6, all of the nucleotides from the RNA strand have sugar puckers that fall between 0°-40°, indicating that they were all in the *C3'-endo* conformation during the simulation. Regarding the DNA strands, all of the nucleotides sugar puckers fall between 120°-180°, indicating that they were all in the *C2'-endo* conformation during the simulation.

The N-glycosidic torsion angle describes the rotation about the glycosidic bond (between the sugar and the base) in nucleic acids. Experiment along with theory anticipated two primary low-energy conformations for the *A-form* and *B-form* duplexes, where the chi (χ) torsion angle, which describes the relative sugar-nucleobase orientation in conventional nucleic acids. Values in the range of +90° to +180° and -90° to -180° belong to the anti-conformation while range of -90° to +90° relate to the *syn*-conformation [46]. The chi (χ) torsion distribution of the monomer nucleotides from both strands of the ASO/RNA duplexes is presented in Figure 5.7 to examine the rigidity of the nucleotide residues across the duplex. Figure 5.7 shows that the monomer nucleotides from the DNA strand have chi (χ) values ranging from -60° to -180° and the residues from the RNA strand have values ranging from -120° to -180°, both of which indicate that the residues are in an anti-conformation typical of *A-form* or *B-form* conformations in duplexes.

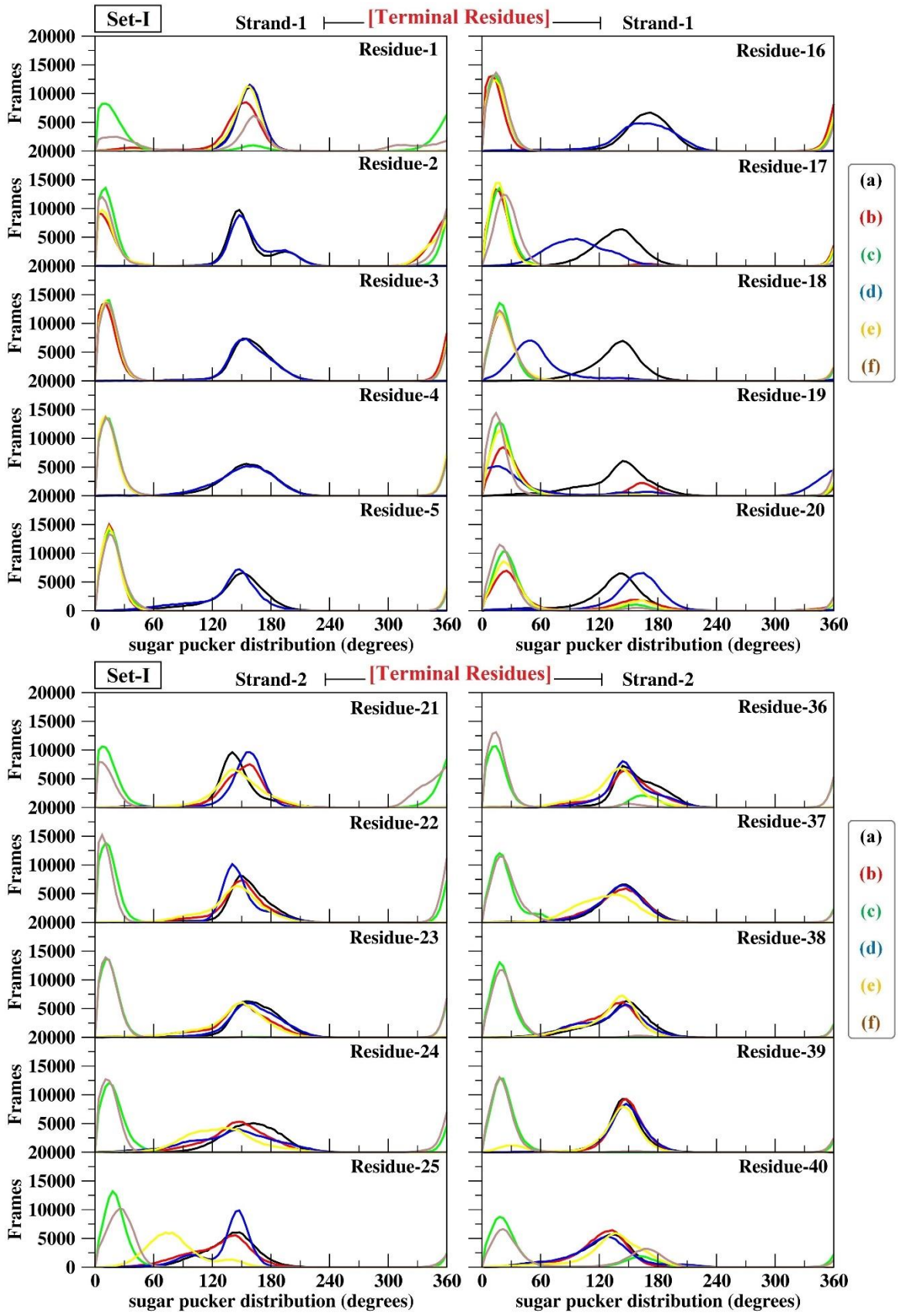
Set-I
Strand-1
[Terminal Residues]
Strand-1
Residue-1
Residue-16
Residue-2
Residue-17
Residue-3
Residue-18
Residue-4
Residue-19
Residue-5
Residue-20
Frames
sugar pucker distribution (degrees)
(a)
(b)
(c)
(d)
(e)
(f)
Set-I
Strand-2
[Terminal Residues]
Strand-2
Residue-21
Residue-36
Residue-22
Residue-37
Residue-23
Residue-38
Residue-24
Residue-39
Residue-25
Residue-40
Frames
sugar pucker distribution (degrees)
(a)
(b)
(c)
(d)
(e)
(f)

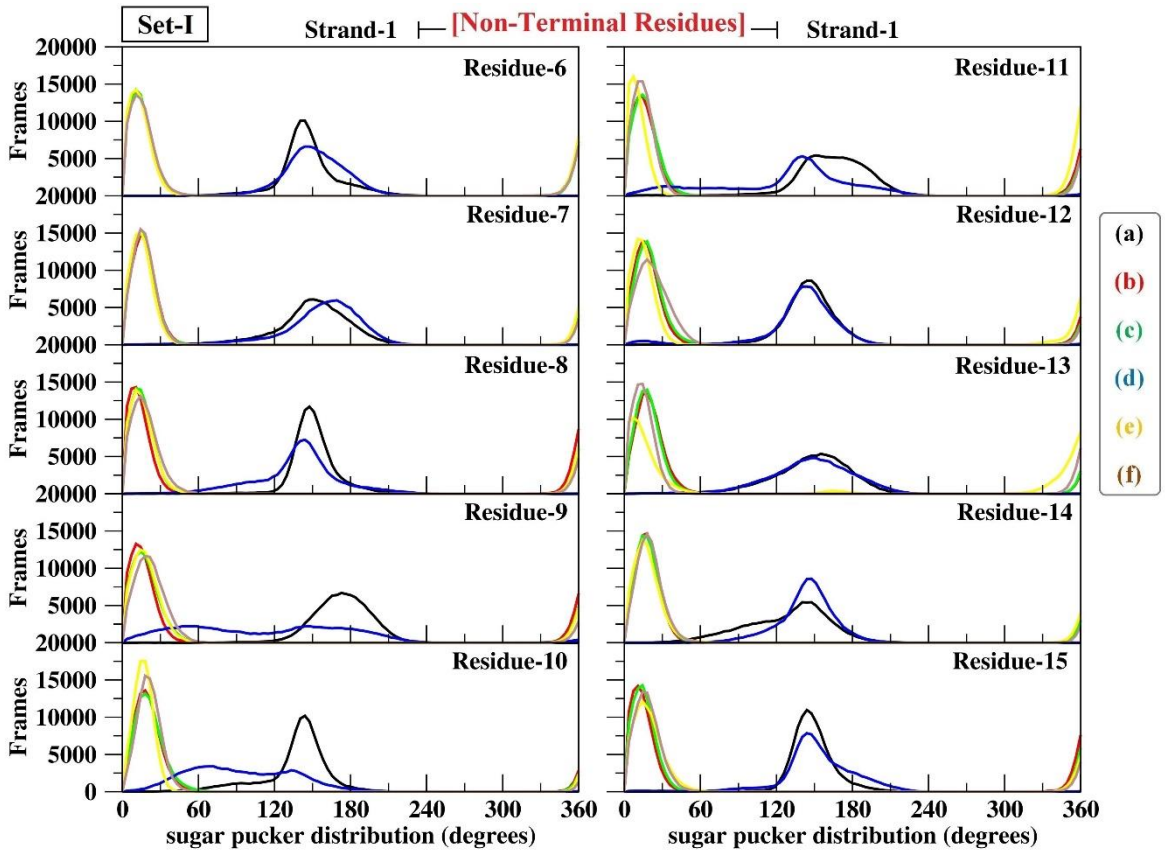
Set-I
Strand-1 [Non-Terminal Residues] Strand-1
Residue-6
Residue-11
Residue-7
Residue-12
Residue-8
Residue-13
Residue-9
Residue-14
Residue-10
Residue-15
Frames
sugar pucker distribution (degrees)
(a)
(b)
(c)
(d)
(e)
(f)

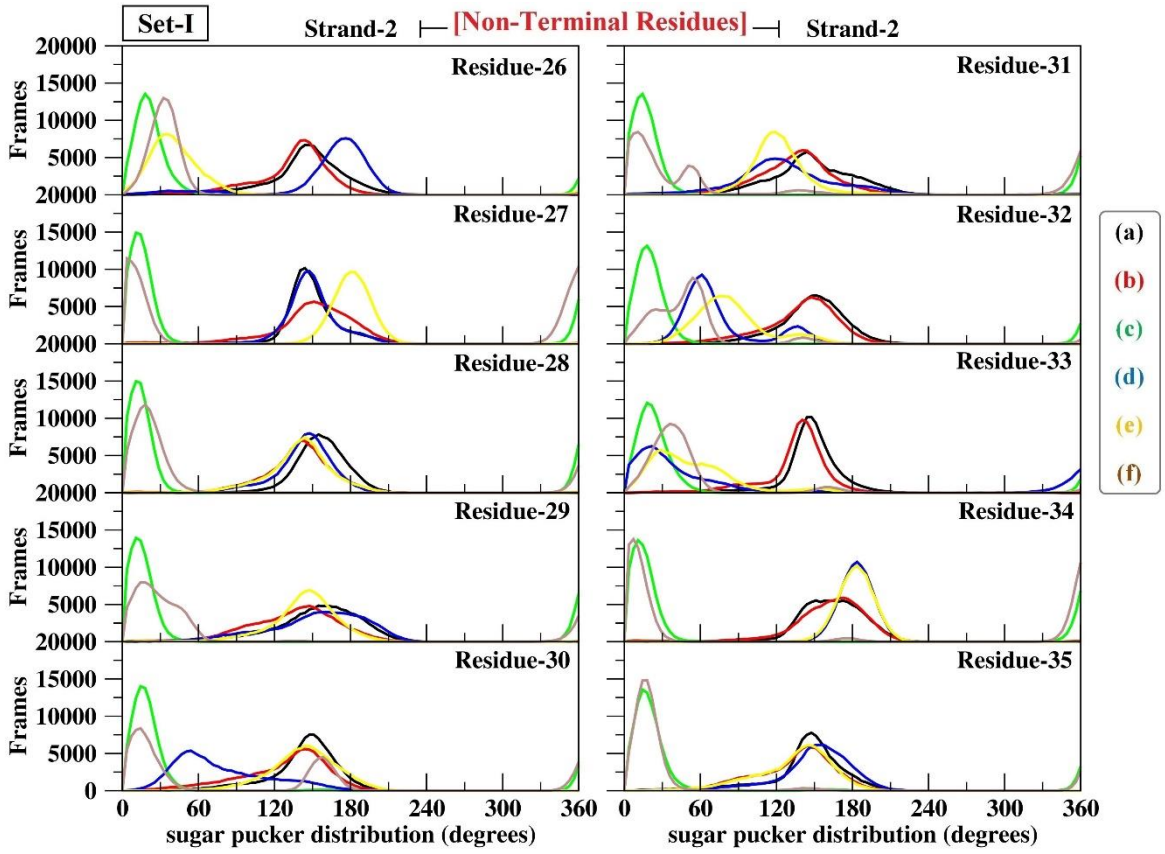
Set-I
Strand-2 [Non-Terminal Residues] Strand-2
Residue-26
Residue-31
Residue-27
Residue-32
Residue-28
Residue-33
Residue-29
Residue-34
Residue-30
Residue-35
Frames
sugar pucker distribution (degrees)
(a)
(b)
(c)
(d)
(e)
(f)

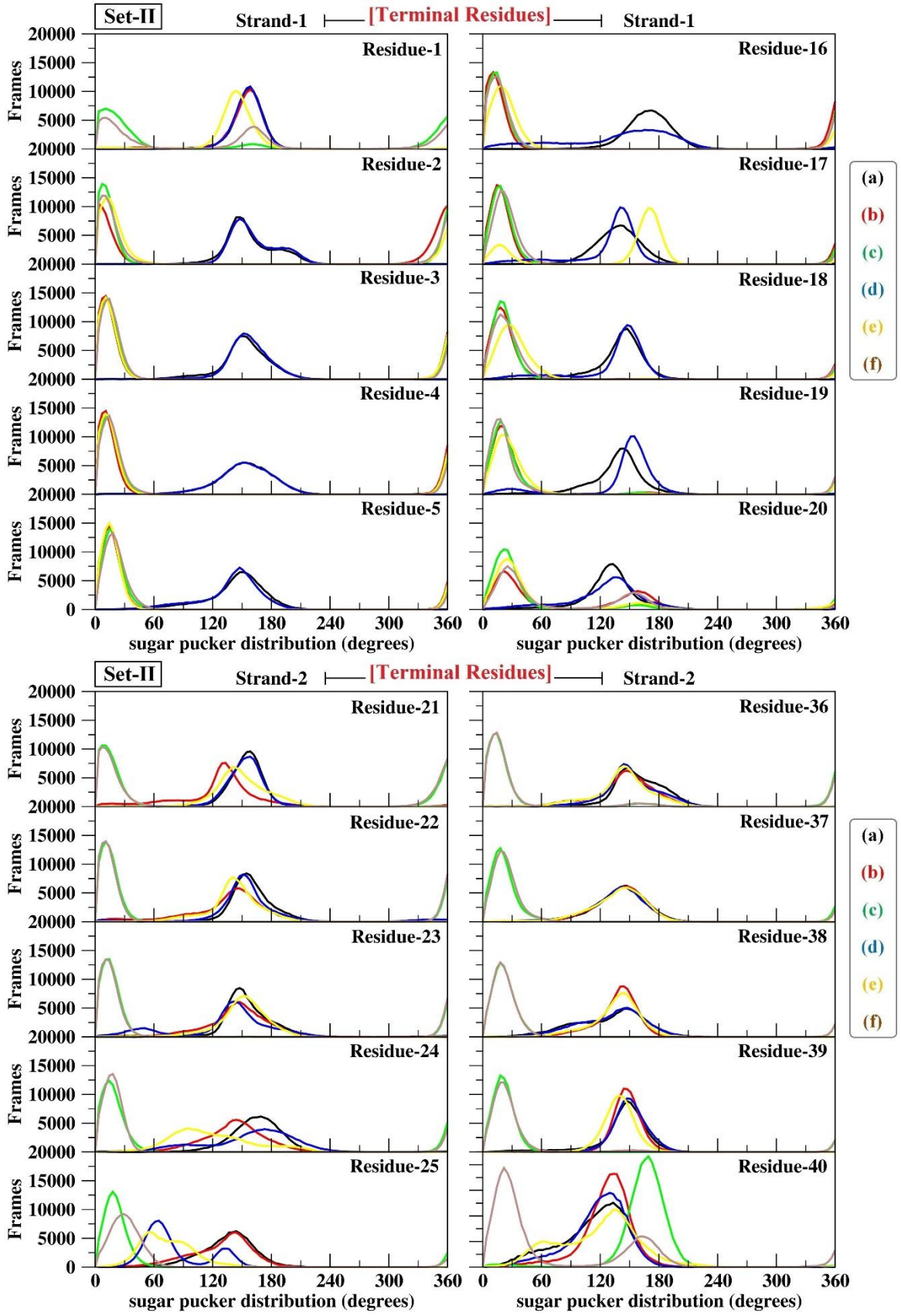
Set-II
Strand-1
[Terminal Residues]
Strand-1
Residue-1
Residue-2
Residue-3
Residue-4
Residue-5
Residue-16
Residue-17
Residue-18
Residue-19
Residue-20
Frames
sugar pucker distribution (degrees)
(a)
(b)
(c)
(d)
(e)
(f)
Set-II
Strand-2
[Terminal Residues]
Strand-2
Residue-21
Residue-22
Residue-23
Residue-24
Residue-25
Residue-36
Residue-37
Residue-38
Residue-39
Residue-40
Frames
sugar pucker distribution (degrees)
(a)
(b)
(c)
(d)
(e)
(f)

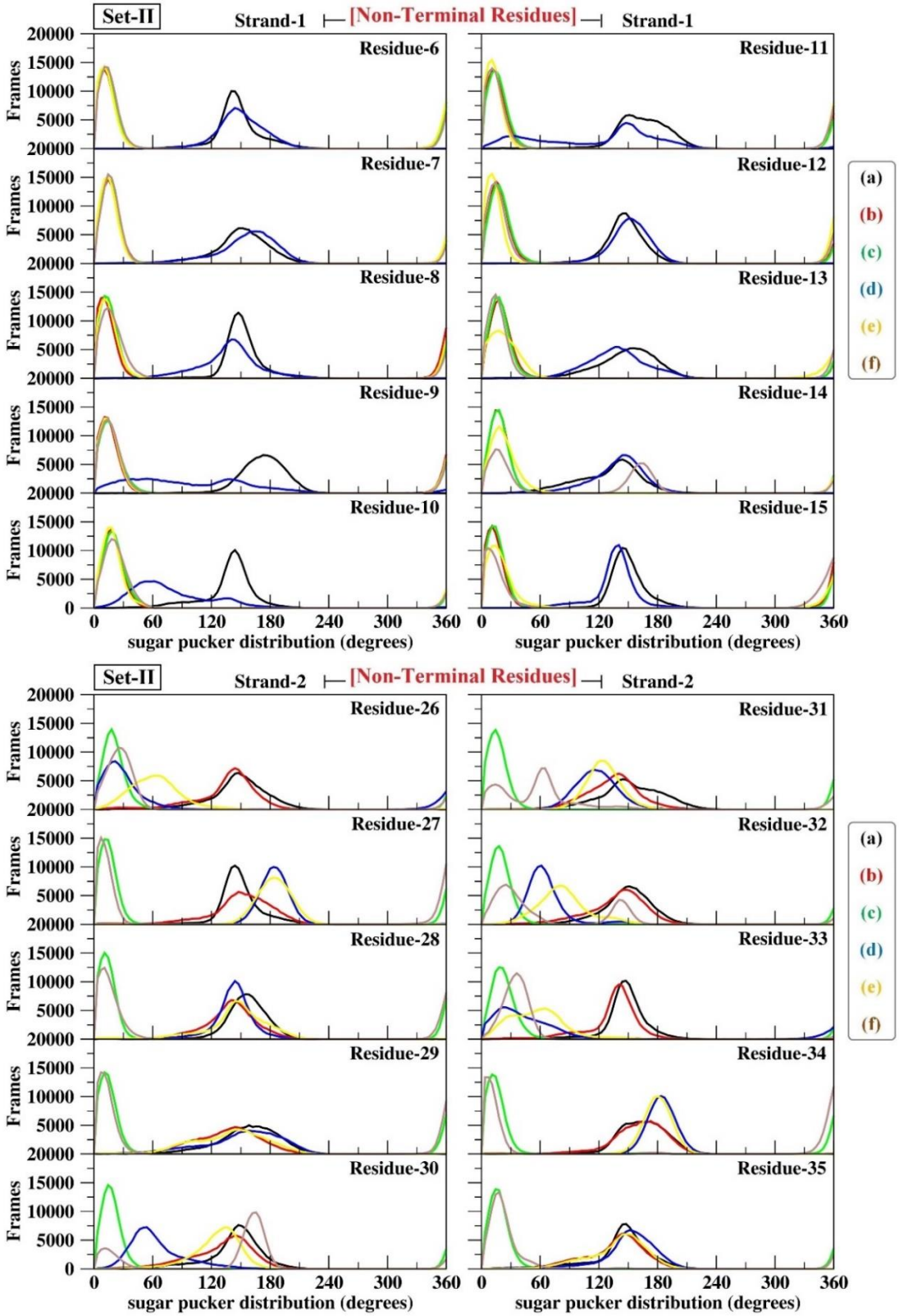

Figure 5.6: Sugar pucker distribution of (a) DNA/DNA (b) RNA/DNA, (c) RNA/RNA, (d) DNA/DNA-RNaseH (e) RNA/DNA-RNaseH and (f) RNA/RNA-RNaseH of simulation trajectories from two data sets [Set-I & Set-II] each simulated for 1 µs simulation time.

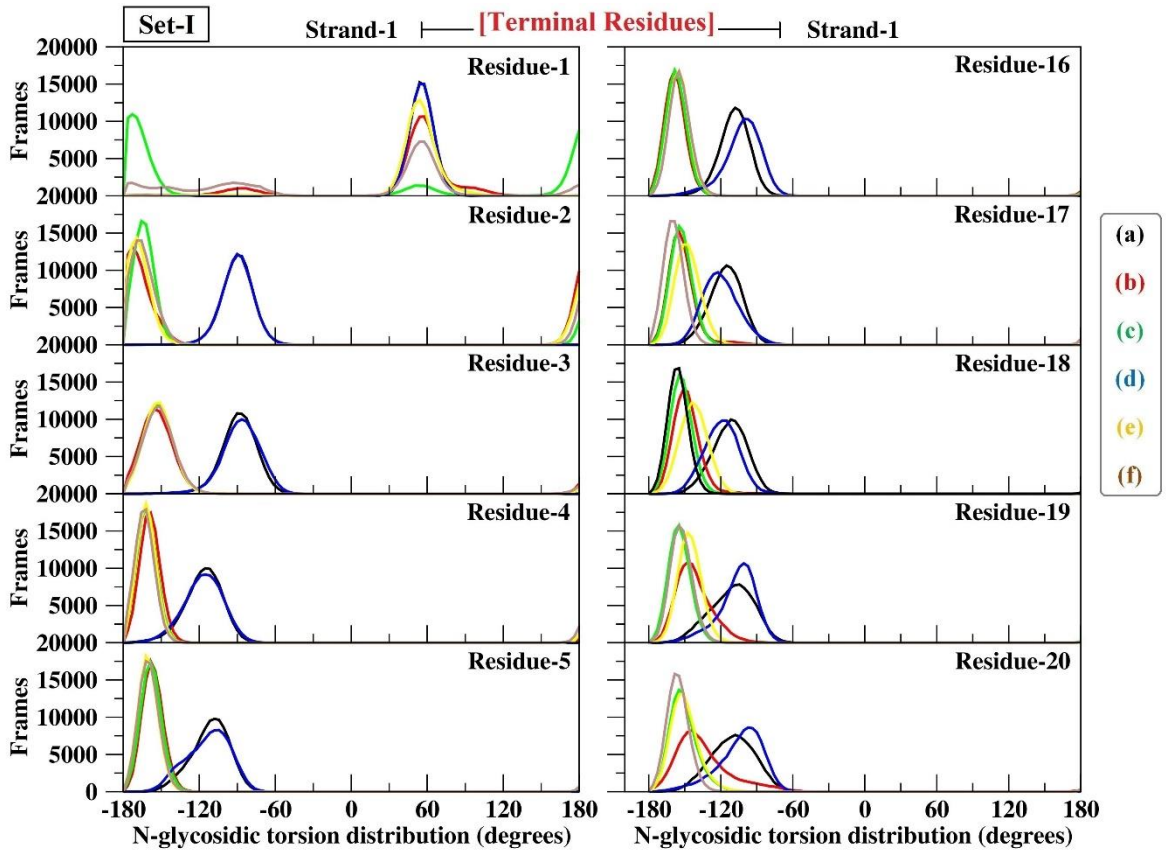
Set-I
Strand-1
[Terminal Residues]
Strand-1
Residue-1
Residue-2
Residue-3
Residue-4
Residue-5
Residue-16
Residue-17
Residue-18
Residue-19
Residue-20
Frames
N-glycosidic torsion distribution (degrees)
(a)
(b)
(c)
(d)
(e)
(f)

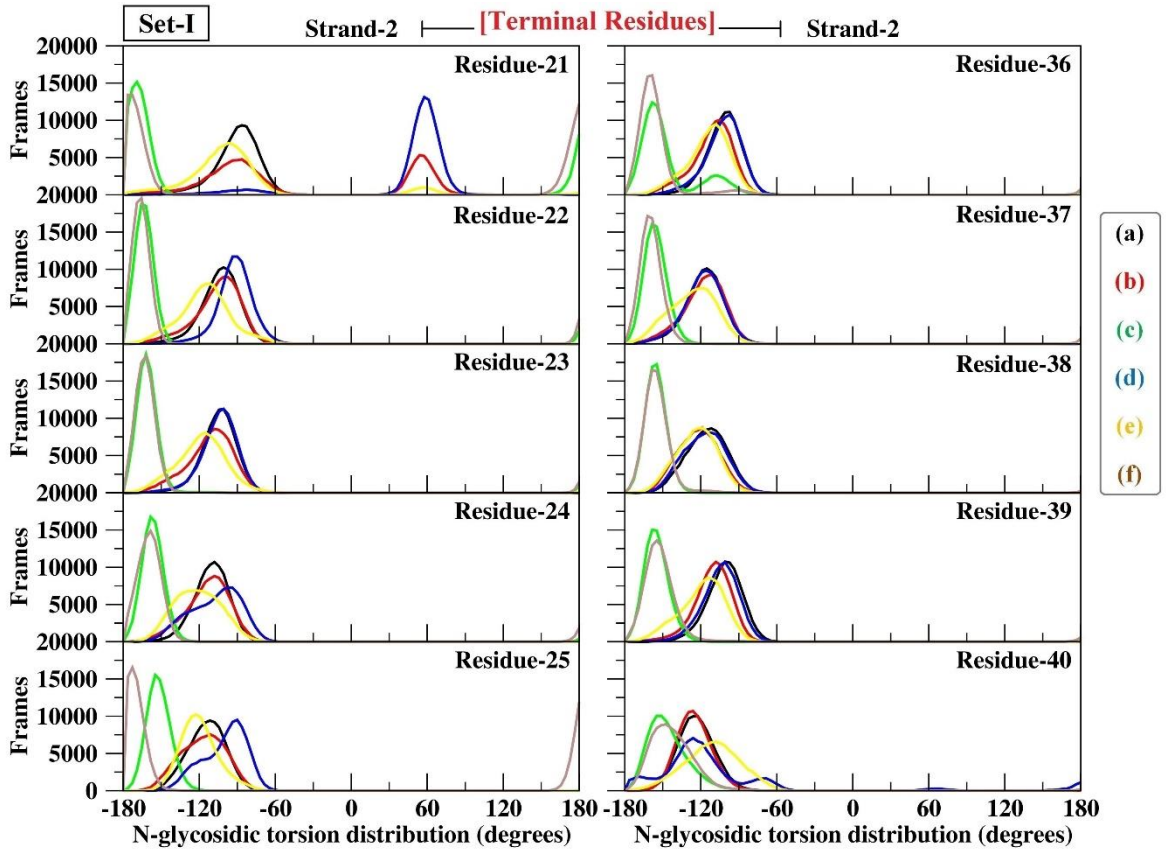
Set-I
Strand-2
[Terminal Residues]
Strand-2
Residue-21
Residue-22
Residue-23
Residue-24
Residue-25
Residue-36
Residue-37
Residue-38
Residue-39
Residue-40
Frames
N-glycosidic torsion distribution (degrees)
(a)
(b)
(c)
(d)
(e)
(f)

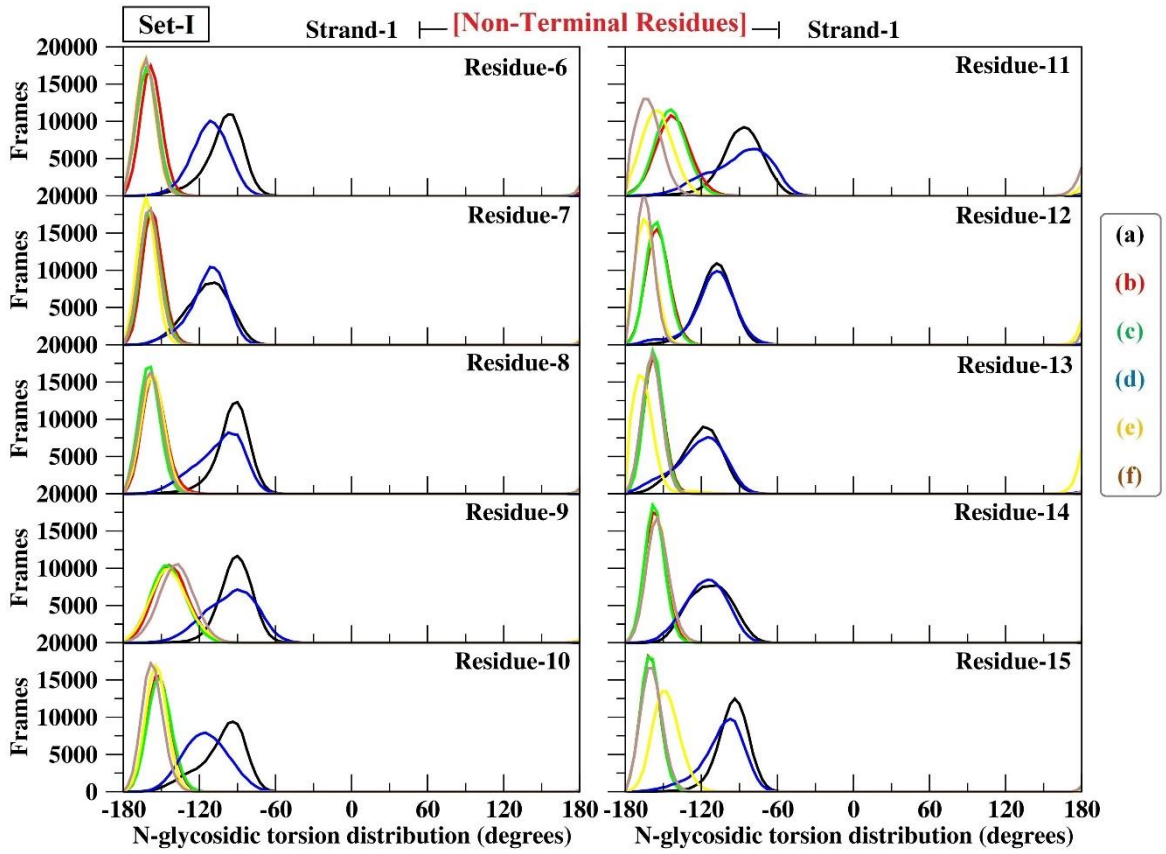
Set-I
Strand-1 [Non-Terminal Residues] Strand-1
Residue-6
Residue-11
Residue-7
Residue-12
Residue-8
Residue-13
Residue-9
Residue-14
Residue-10
Residue-15
Frames
20000
15000
10000
5000
0
-180 -120 -60 0 60 120 180
N-glycosidic torsion distribution (degrees)
(a)
(b)
(c)
(d)
(e)
(f)

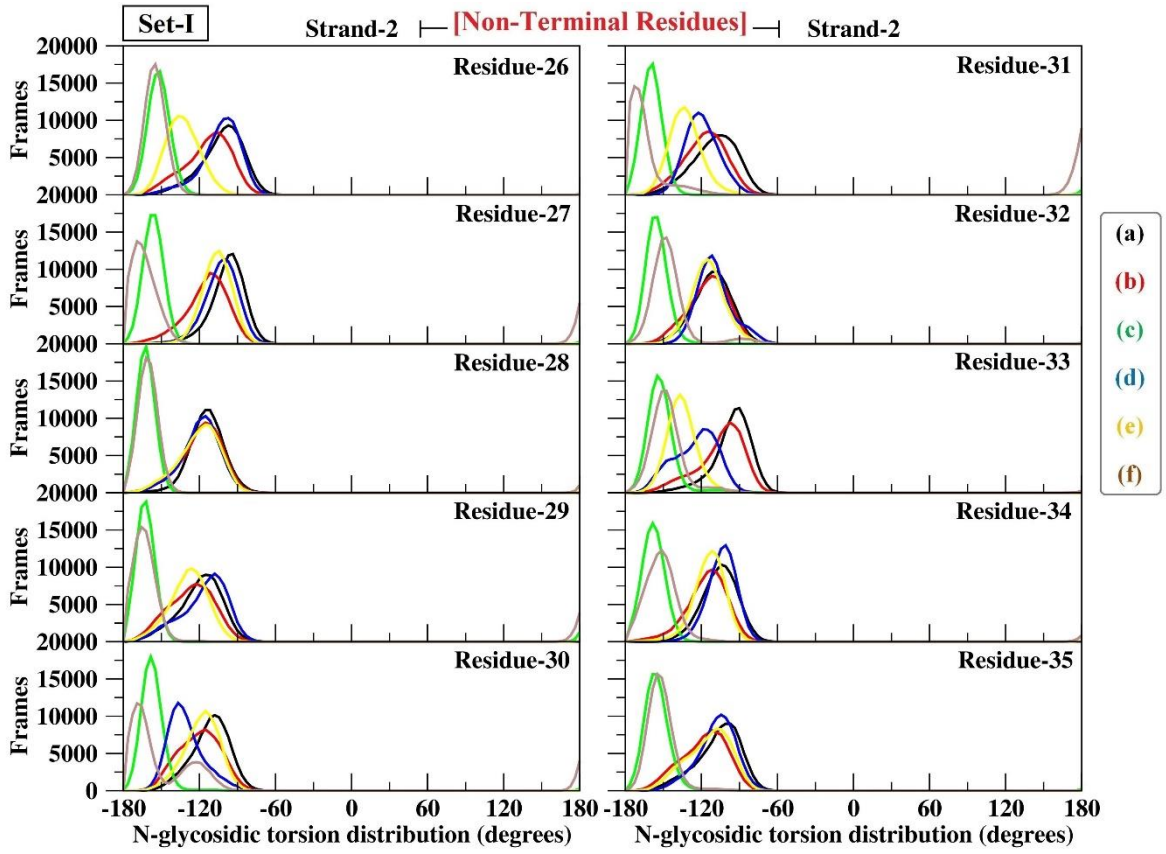
Set-I
Strand-2 [Non-Terminal Residues] Strand-2
Residue-26
Residue-31
Residue-27
Residue-32
Residue-28
Residue-33
Residue-29
Residue-34
Residue-30
Residue-35
Frames
20000
15000
10000
5000
0
-180 -120 -60 0 60 120 180
N-glycosidic torsion distribution (degrees)
(a)
(b)
(c)
(d)
(e)
(f)

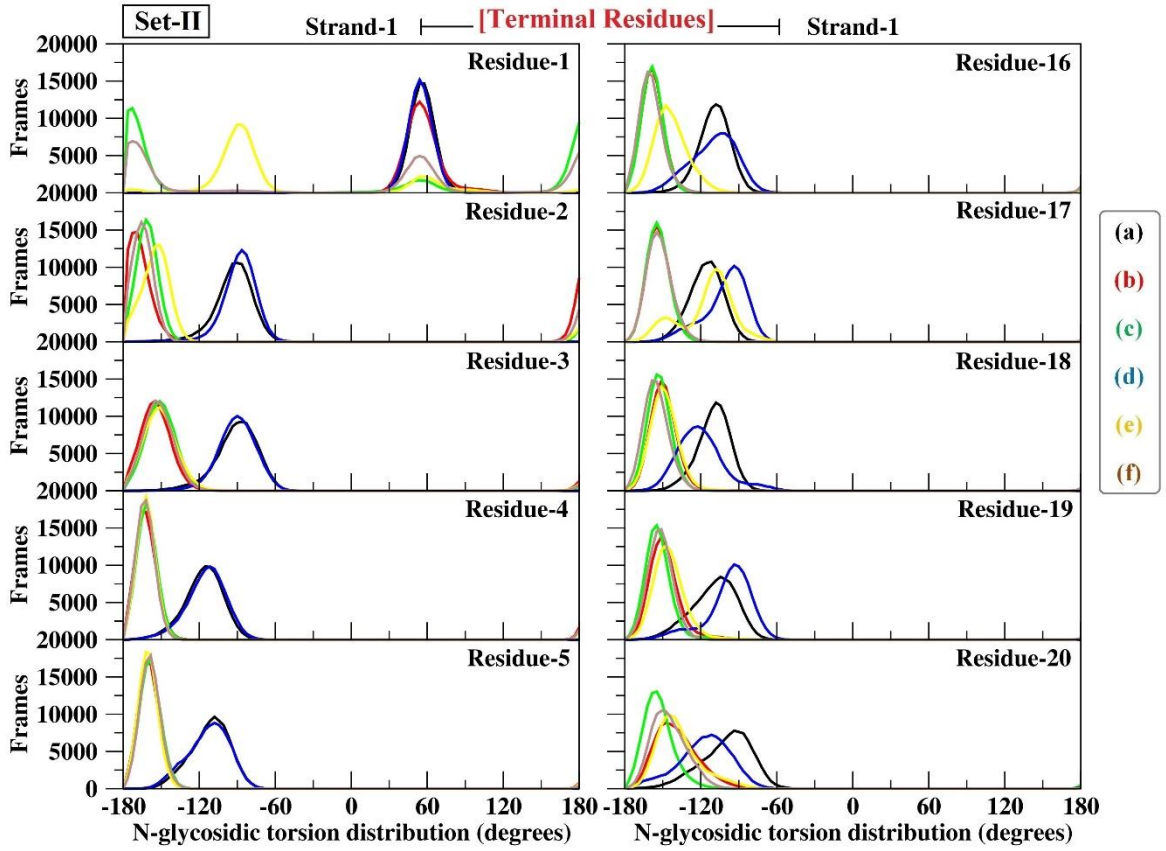
Set-II
Strand-1
[Terminal Residues]
Strand-1
Residue-1
Residue-2
Residue-3
Residue-4
Residue-5
Residue-16
Residue-17
Residue-18
Residue-19
Residue-20
Frames
N-glycosidic torsion distribution (degrees)
(a)
(b)
(c)
(d)
(e)
(f)

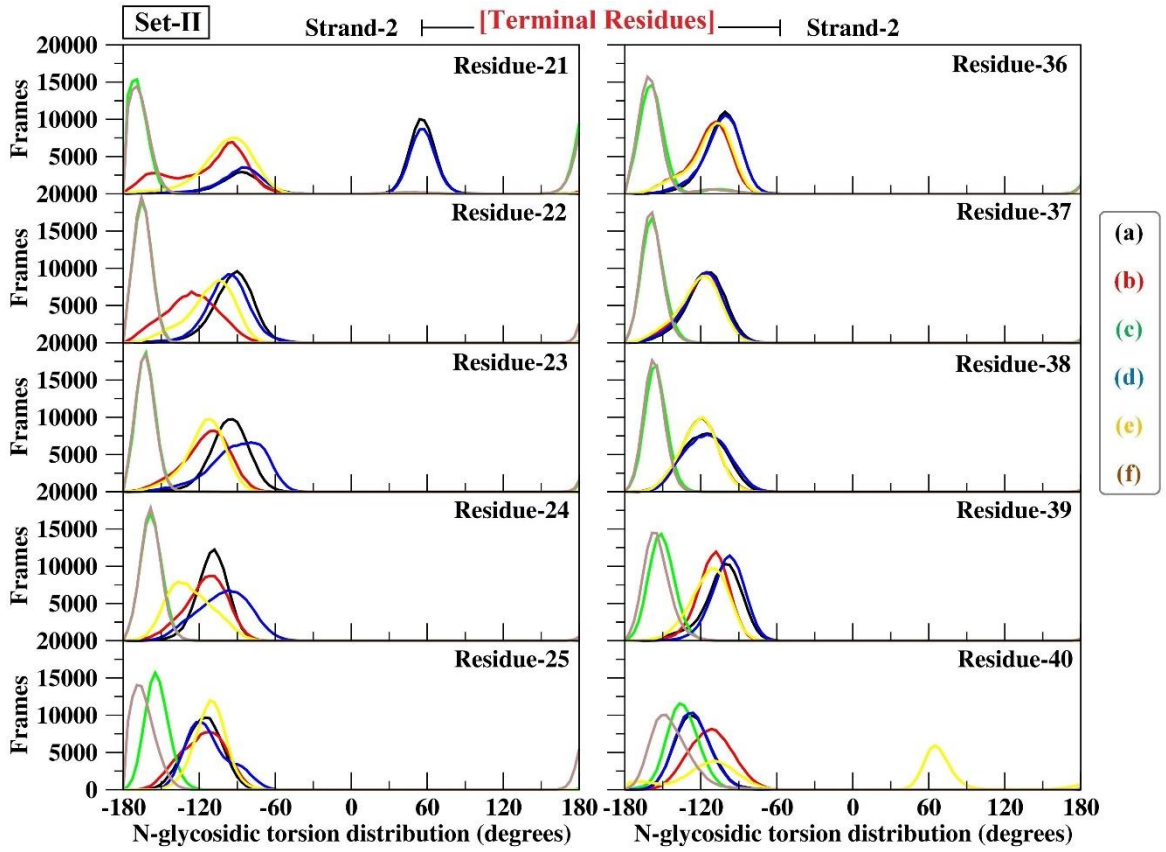
Set-II
Strand-2
[Terminal Residues]
Strand-2
Residue-21
Residue-22
Residue-23
Residue-24
Residue-25
Residue-36
Residue-37
Residue-38
Residue-39
Residue-40
Frames
N-glycosidic torsion distribution (degrees)
(a)
(b)
(c)
(d)
(e)
(f)

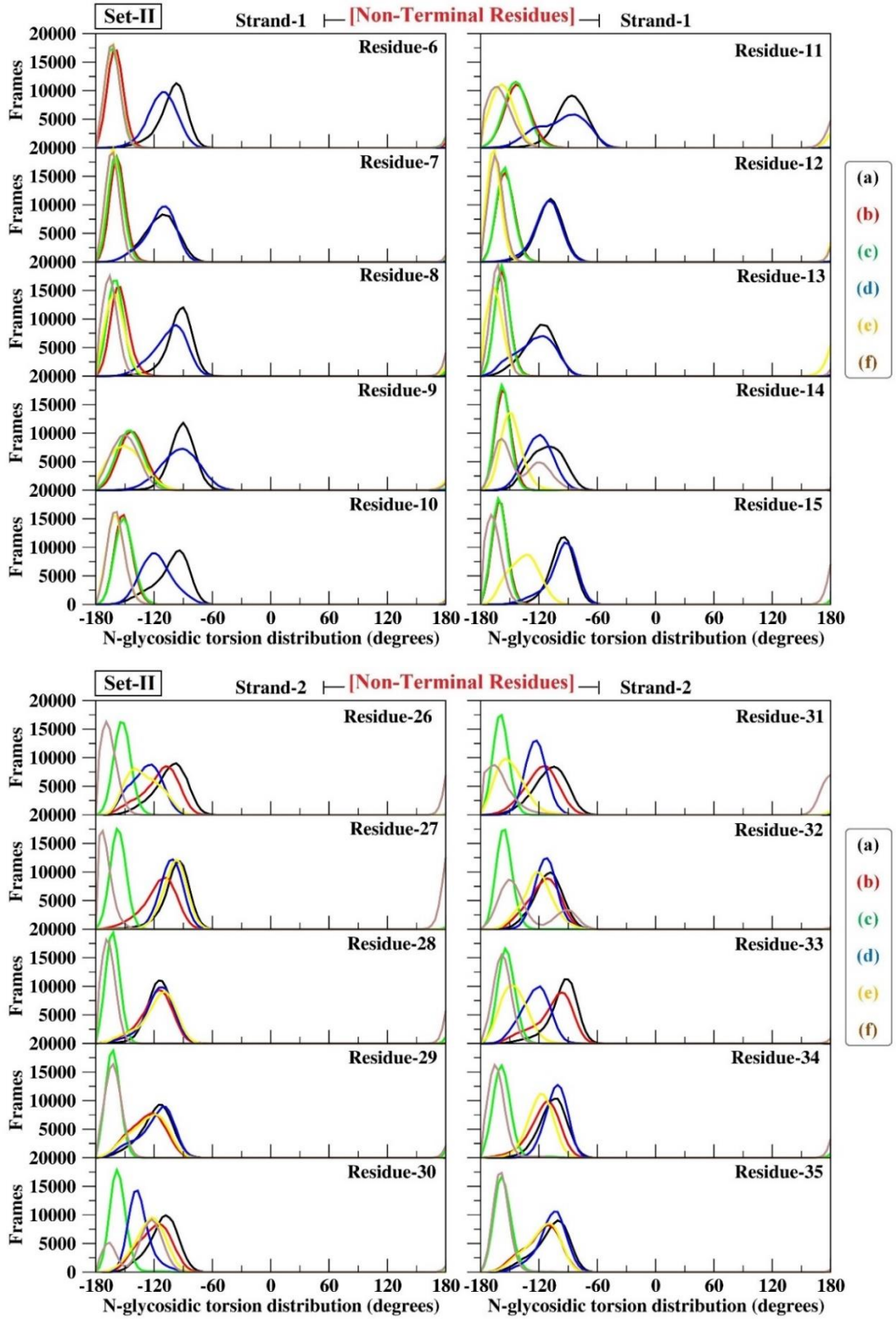

Figure 5.7: N-glycosidic torsion distribution of (a) DNA/DNA (b) RNA/DNA, (c) RNA/RNA, (d) DNA/DNA-RNaseH (e) RNA/DNA-RNaseH and (f) RNA/RNA-RNaseH of simulation trajectories from two data sets [Set-I & Set-II] each simulated for 1 μs simulation time.

5.3.4. Backbone flexibility of the DNA/DNA, RNA/DNA and RNA/RNA duplexes

Human RNase H identification of antisense duplexes is greatly influenced by the flexibility of the sugar-phosphate backbone. Therefore, backbone flexibility of duplexes significantly contributes to the transmission of dominant antisense activity. Directionality and flexibility of the nucleotides throughout the duplex are provided by the sugar-phosphate backbone of nucleic acid duplexes. To explore the influence of the duplex backbone flexibility residue wise RMSF of backbone heavy atoms calculated for each nucleotide from both the nucleic acid strands are plotted in Figure 5.8. RMSF plots of the RNaseH alone are plotted in Figure 5.9. In comparison to the non-terminal residues, the terminal residues typically exhibit higher flexibility. Accordingly, terminal residues of the duplexes demonstrated higher fluctuations compared to the non-terminal residues. Duplexes may have tried to adjust more during simulation Set-I as the nucleotide residues are seen to fluctuate more in case of simulation Set-I compared to simulation Set-II.

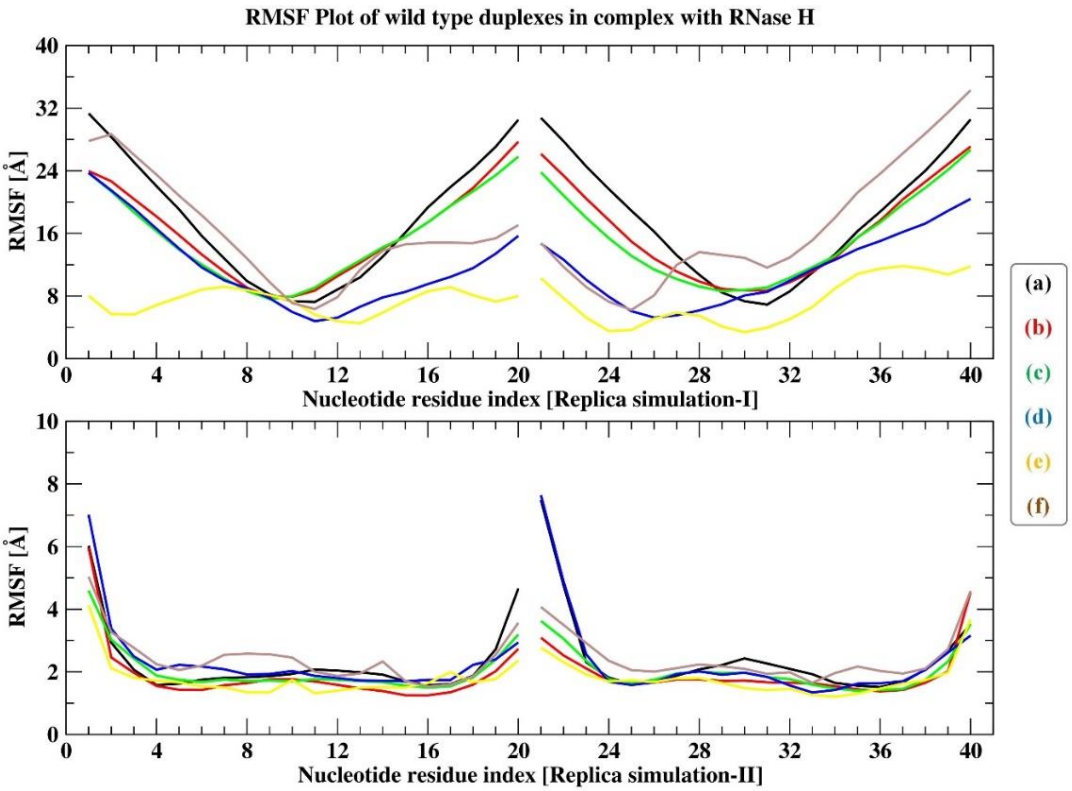

Figure 5.8: RMSF plot of (a) DNA/DNA (b) RNA/DNA, (c) RNA/RNA, (d) DNA/DNA-RNaseH (e) RNA/DNA-RNaseH and (f) RNA/RNA-RNaseH of simulation trajectories from two data sets [Set-I & Set-II] each simulated for 1 μs simulation time.

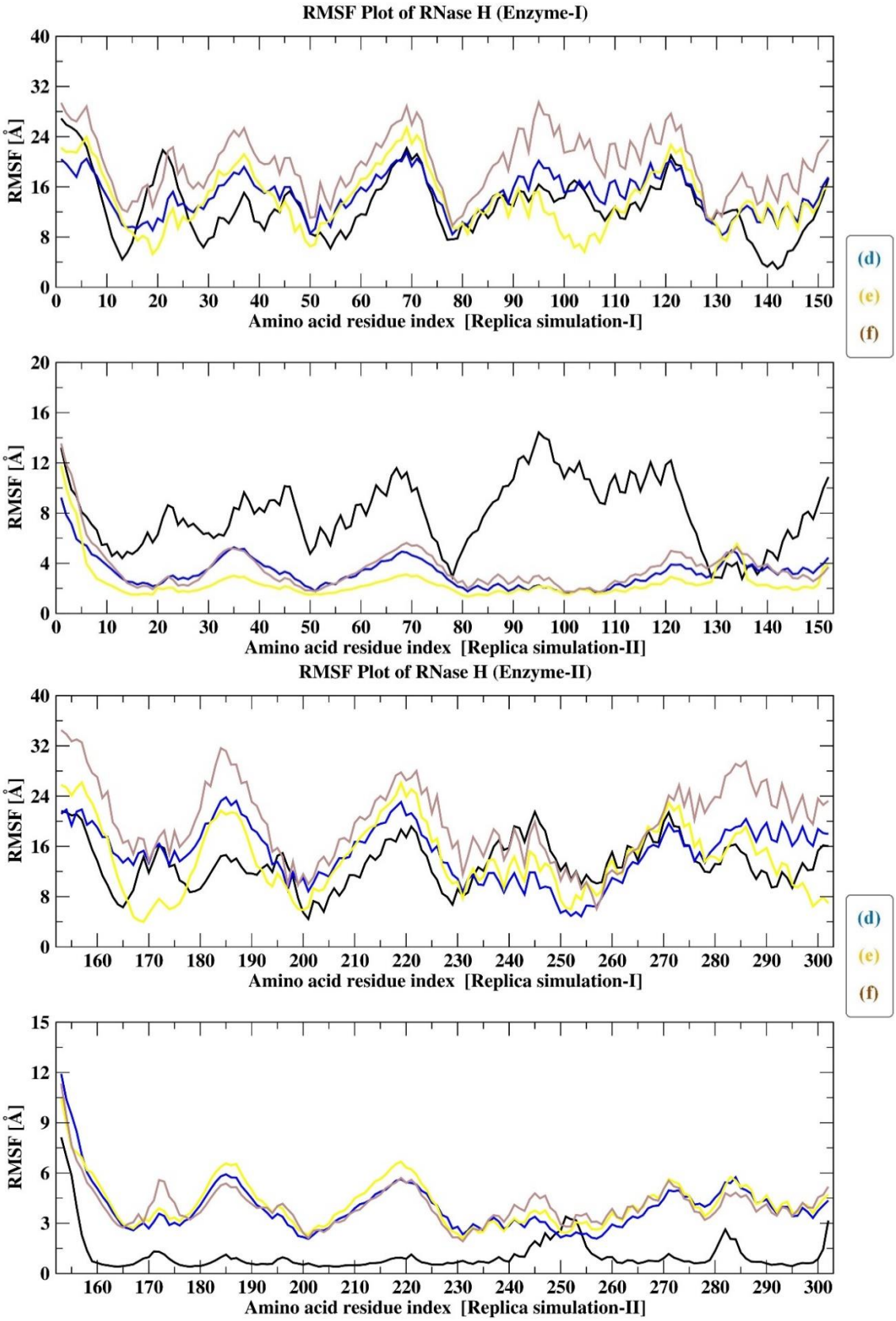

Figure 5.9: RMSF plots of the RNase H alone from the (d) DNA/DNA-RNaseH (e) RNA/DNA-RNaseH and (f) RNA/RNA-RNaseH complexes of simulation trajectories from two data sets [Set-I & Set-II] each simulated for 1 μs simulation time.

5.3.5. H-Bond interactions, Base-pairing, Base-stacking and Helix-turning of the DNA/DNA, RNA/DNA and RNA/RNA duplexes

Noting the importance of the amino acid residues at the active site of the catalytic domain; the acceptor-donor residues, average bond distances, average bond angles, bond residence frames for the complexes (d)-(f) with HBond interactions > 50 % occupancies from the simulation trajectories from both the data sets [Set-I & Set-II] were studied. H-Bond parameters of duplexes are in well agreement with the crystal data values corresponding to the *A*-form or the *B*-form duplex structure of the DNAs and RNAs [47]. Amino acid residues from the RNase H catalytic domain forming HBond interactions with the duplexes for more than 50% residence time has been sorted and plotted in Table 5.1. It was observed that some common amino acid residues as ASN-19, ARG-47, TRP-93, SER-101, ILE-107, TRP-243, SER-251 at the active site of RNase H interacted with all the three wild type DNA/DNA, RNA/DNA and RNA/RNA duplexes. Thus, apart from the aspartate and glutamate amino residues a few amino acid residues as ASN-19, ARG-47, TRP-93, SER-101, ILE-107, TRP-243, SER-251 are stabilising the duplexes at the active site of the RNase H.

Table 5.1: Participating residues of (d) DNA/DNA-RNaseH (e) RNA/DNA-RNaseH and (f) RNA/RNA-RNaseH complexes with HBond interactions > 50 % occupancies of simulation trajectories from two data sets [Set-I & Set-II] each simulated for 1 µs simulation time.

ASO/RNA-RNaseH Systems	Acceptor Residues	Donor Residues
DNA/DNA-RNaseH	GLN_51, DC_315, DC_321, DT_327, DC_328, DA_329, DG_330, DT_332, DG_333, DT_334, DC_335, DG_336	SER_17, ASN_19, ARG_47, TRP_93, SER_101, ILE_107, ARG_197, TRP_243, THR_250, SER_251, ILE_257, ASN_258, ARG_296, DG_333
RNA/DNA-RNaseH	CYS_16, GLN_51, C_315, U_316, U_320, DC_328, DA_329, DT_332, DT_334, DC_335, DG_336	SER_17, ASN_19, ARG_47, THR_49, GLN_51, TRP_93, SER_101, ILE_107, ARG_146, ASN_228, TRP_243, SER_251, ILE_257, C_314, DG_333
RNA/RNA-RNaseH	ASN_19, C_314, C_315, U_327, C_328, A_329, U_334, C_335, G_336	ASN_19, ARG_47, TRP_93, SER_101, ILE_107, ASN_108, ARG_146, ARG_197, TRP_243, SER_251, ASN_258, G_331

5.3.6. SASA and MM-GBSA of the DNA/DNA, RNA/DNA and RNA/RNA duplexes

Research on protein folding and drug-protein stability has long recognized solvent accessible surface area (SASA) and MM-GBSA binding free energy as crucial factors to understand the underlying chemistry [48]. Studying the SASA and MM-GBSA free energies of the wild type duplexes will therefore help us better comprehend the solvation pattern including the stability of the duplexes. As a result, the SASA and MM-GBSA binding free energy values for each of the duplexes were calculated taking into account the complete simulation trajectory presented in Table 5.2 and Table 5.3, respectively. A duplex's nucleotide residues can be categorized as buried or exposed based on SASA values. The greater the SASA values, the greater the surface area of contact between the duplexes and the water molecules, indicating duplexes increased solubility in water. Accordingly, results of SASA values in Table 5.2 revealed that for the particular nucleic acid sequence, solvation of the wild type DNA/DNA, RNA/DNA, RNA/RNA duplexes in presence of the RNase H were higher than the DNA/DNA, RNA/DNA, RNA/RNA duplexes without the RNase H for both Set-I & Set-II simulation trajectories. This implies that the duplexes were very much available to the nearby solvent environment upon interaction with the RNase H influencing their binding capacity with the solvent environment, which may have led to increased SASA values post complexation.

Table 5.2: SASA of (a) DNA/DNA (b) RNA/DNA, (c) RNA/RNA, (d) DNA/DNA-RNaseH (e) RNA/DNA-RNaseH and (f) RNA/RNA-RNaseH of simulation trajectories from two data sets [Set-I & Set-II] each simulated for 1 μs simulation time.

Name Code	Replica Simulation-I		Replica Simulation-II	
	$SASA_{(ASO/RNA)}$	$SASA_{RNaseH}$	$SASA_{(ASO/RNA)}$	$SASA_{RNaseH}$
DNA/DNA	3538.41	-	3531.31	-
RNA/DNA	3690.69	-	3645.11	-
RNA/RNA	3605.76	-	3636.02	-
DNA/DNA-RNaseH	5504.74	14227.48	5565.14	13737.74
RNA/DNA-RNaseH	5598.77	13948.03	5496.58	13727.87
RNA/RNA-RNaseH	5199.94	13619.40	5691.77	13971.66

MM-GBSA binding free energy values of all the duplexes for the entire simulation trajectory were computed with the equation:

$$\Delta G_{Binding} = G_{Complex} - G_{RNaseH} - G_{Duplex}$$

Herein, the energies were calculated considering the RNase H as the target protein receptor, the wild type duplexes as the binding ligand and the wild type duplexes in complex with the RNase H as the receptor-ligand complex.

In the RNase H dependent mechanism of antisense activity, RNase H is activated by an RNA/DNA duplex which specifically cleaves the RNA strand from the RNA/DNA duplex in a targeted manner. Thus, it is expected of the RNA/DNA duplex to be more stable at the active site of RNase H. Accordingly, the binding free energy change (ΔG**)** is the highest for the RNA/DNA-RNaseH complex and lowest for DNA/DNA-RNaseH and RNA/RNA-RNaseH complex being the intermediate. A slight difference in binding energy between RNA/DNA-RNaseH and RNA/RNA-RNaseH complexes might be attributed to the structural and chemical differences between RNA and DNA molecules. As seen in Table 5.3, free energy (G) of RNase H has nearly identical energy values and free energy of the wild type duplexes varied depending on the type of nucleic acids. Free energy of RNA/RNA duplex is highest and DNA/DNA is lowest with RNA/DNA duplex being the intermediate. RNA/RNA duplex is more stable than DNA/RNA duplex. This might be because of the presence of the 2'-hydroxyl group in RNA, which can participate in additional hydrogen bonding interactions. Thus, RNA/DNA hybrids typically have slightly lower stability compared to RNA/RNA non-hybrids due to differences in base pairing. RNA/DNA hybrids hence may exhibit greater structural flexibility compared to RNA/RNA non-hybrids due to differences in backbone conformation and flexibility between RNA and DNA molecules. This flexibility of RNA/DNA duplex could affect the overall stability of the RNA/DNA-RNaseH complex and contribute to the observed difference in binding energy. Additionally, the enzyme's active site may interact differently with the two types of hybrids, influencing the overall stability of the complexes. RNaseH might tolerate certain mismatches in the RNA/DNA hybrid region more effectively than in RNA/RNA non-hybrids. This tolerance can contribute to RNaseH to have different affinities or specificities for RNA/DNA hybrids compared to RNA/RNA non-hybrids, leading to differences in binding energy in the RNA/DNA-RNaseH complex compared to the RNA/RNA-RNaseH. Overall, the slight difference in

binding energy between RNA/DNA-RNaseH and RNA/RNA-RNaseH systems likely arises from a combination of these factors, including the chemical properties of RNA and DNA molecules, the tolerance of mismatches, structural flexibility, and enzyme specificity.

Regarding the lower stability of the DNA/DNA-RNaseH, RNase H enzymes have evolved to specifically recognize RNA/DNA hybrids rather than DNA/DNA duplexes. The active site of RNase H is optimized to cleave the RNA strand in RNA/DNA hybrids, which is complementary to the DNA strand. DNA/DNA duplexes do not have the same level of recognition and interaction with the enzyme, leading to lower stability at the active site. DNA also lacks the 2'-hydroxyl group present in RNA. This hydroxyl group in RNA molecules can form additional hydrogen bonds, enhancing the stability of RNA-containing hybrids like RNA/DNA or RNA/RNA duplexes. The absence of this group in DNA reduces the number of potential H-bonding interactions, resulting in lower stability.

Thus, the MM-GBSA binding energies of the wild type duplexes estimated for the entire simulation trajectory predicted RNA/DNA duplex to have higher affinity or is more stable at the active site of the RNase H catalytic domain, for both Set-I & Set-II simulation trajectories.

Table 5.3: MM-GBSA of (d) DNA/DNA-RNaseH (e) RNA/DNA-RNaseH and (f) RNA/RNA-RNaseH complexes of simulation trajectories from two data sets [Set-I & Set-II] each simulated for 1 μs simulation time.

Name Code	Replica Simulation-I			
	$G_{(Duplexes)-RNaseH}$	G_{RNaseH}	$G_{Duplexes}$	ΔG (kcal/ mol)
DNA/DNA-RNaseH	-15173.24	-7787.56	-7246.22	-139.47
RNA/DNA-RNaseH	-15626.02	-7757.00	-7594.08	-274.94
RNA/RNA-RNaseH	-15902.64	-7758.15	-7893.04	-251.44
Name Code	**Replica Simulation-II**			
	$G_{(Duplexes)-RNaseH}$	G_{RNaseH}	$G_{Duplexes}$	ΔG (kcal/ mol)
DNA/DNA-RNaseH	-15189.22	-7799.82	-7227.32	-162.08
RNA/DNA-RNaseH	-15609.30	-7770.04	-7590.48	-248.79
RNA/RNA-RNaseH	-15899.78	-7771.63	-7884.81	-243.34

5.4. Summary

Simulations were conducted to study the structure and dynamic properties of a set of 20-mer wild-type DNA/DNA, RNA/DNA, RNA/RNA duplexes complexed with a Human RNase H catalytic domain. Replica sets of MD simulations accounting to two data sets (Set-I & Set-II) were performed, each simulated for 1 μs simulation time. Structures of the duplexes obtained at the 500th ns and 1000th ns were maintaining stable *Watson-Crick* base-pairing, base-stacking pattern and ideal helix-turning for both the sets of simulation. Stability of the duplexes throughout the simulation trajectories were studied by observing their RMSD plots. The duplexes were fluctuating potentially within and around a range of 2 to 6 Å RMSD values. RMSD of DNA/DNA and DNA/DNA-RNaseH is slightly higher. RMSD data over time for the wild type duplexes showed that duplex stability is well retained for the full simulation trajectory for both sets of simulation.

The duplexes preferred their natural organizations where RNA residues were *A-type* with *C3'-endo* sugar puckering and DNA residues were *B-type* with *C2'-endo* sugar puckering maintaining stable *anti*-conformations typical of *A-form* or *B-form* conformations in duplexes [49-51]. Intra-strand distances of the sugar phosphate backbone exhibited clear distinction for the DNA, RNA residues from the homoduplexes where the DNA residues exhibited intra-strand distances greater than RNA residues as per expectation. In case of the hybrid duplexes, residues are seen to fluctuate more although no residue exhibited intra-strand distance >7 Å. Inter-strand distances of the wild type duplexes are lying in the acceptable range of 19-20 Å, for both the sets of simulations. Nucleotide residues from the RNA strand have sugar puckers in the *C3'-endo* conformation and nucleotide residues from the DNA strand have sugar puckers in the *C2'-endo* conformation. Monomer nucleotides from the wild-type duplexes all are in anti-conformation typical of *A-form* or *B-form* conformations in duplexes. Compared to the non-terminal residues, terminal residues of the duplexes demonstrated high fluctuations and similar pattern of flexibility throughout the residues. One important finding includes the HBond interactions which revealed a few common amino acid residues ASN-19, ARG-47, TRP-93, SER-101, ILE-107, TRP-243, and SER-251 located at the active site of RNase H were found to interact with all three the wild-type duplexes. Henceforth, this research has predicted the critical amino acid residues stabilizing the wild type duplexes at the active site of RNase H, throughout the simulation time.

For the particular nucleic acid sequence, solvation of the wild type duplexes in presence of the RNase H was higher than the bare wild type duplexes without the RNase H. This suggests that the duplexes were highly accessible to the adjacent solvent environment following engagement with the RNase H, which may have affected their ability to bind to the solvent environment and possibly caused a rise in SASA values after complexation, affecting their antisense activity. In the RNase H dependent mechanism of antisense activity, RNase H is activated by the RNA/DNA duplex which specifically cleaves the RNA strand from the RNA/DNA duplex. Thus, it is expected of the RNA/DNA duplex to be more stable at the active site of RNase H. MM-GBSA binding energies of the wild type duplexes estimated for the entire simulation trajectory predicted RNA/DNA duplex to have higher affinity or is more stable at the active site of the RNase H catalytic domain. Given that DNA homo duplexes are less stable compared to RNA homo duplexes and RNA/DNA hybrid duplexes in nature it was observed that MM-GBSA binding energies estimated for the entire simulation trajectory predicted free energy of RNA/RNA is highest and DNA/DNA is lowest with RNA/DNA being the intermediate.

Bibliography

[1] Dias, N., and Stein, C. A. Antisense oligonucleotides: basic concepts and mechanisms. *Molecular cancer therapeutics*, 1(5):347-355, 2002.

[2] Kurreck, J. Antisense technologies: improvement through novel chemical modifications. *European journal of biochemistry*, 270(8): 1628-1644, 2003.

[3] Chan, J. H., Lim, S., and Wong, W. F. Antisense oligonucleotides: from design to therapeutic application. *Clinical and experimental pharmacology and physiology*, 33(5-6): 533-540, 2006.

[4] Saonere, J. A. Antisense therapy, a magic bullet for the treatment of various diseases: present and future prospects. *J Med Genet Genom*, *3*(5): 77-83, 2011.

[5] Le Calvez, H., Yu, M., and Fang, F. Biochemical prevention and treatment of viral infections–A new paradigm in medicine for infectious diseases. *Virology Journal*, *1*:1-6. 2004.

[6] Takei, Y., Kadomatsu, K., Yuzawa, Y., Matsuo, S., and Muramatsu, T. A small interfering RNA targeting vascular endothelial growth factor as cancer therapeutics. *Cancer research*, 64(10): 3365-3370, 2004.

[7] Gong, M., Lu, Z., Fang, G., Bi, J., and Xue, X. A small interfering RNA targeting osteopontin as gastric cancer therapeutics. *Cancer letters*, *272*(1):148-159, 2008.

[8] Stein, C. A., and Castanotto, D. FDA-approved oligonucleotide therapies in 2017. *Molecular Therapy*, *25*(5): 1069-1075, 2017.

[9] Silva, A. C., Lobo, D. D., Martins, I. M., Lopes, S. M., Henriques, C., Duarte, S. P., ... and Pereira de Almeida, L. Antisense oligonucleotide therapeutics in neurodegenerative diseases: the case of polyglutamine disorders. *Brain*, *143*(2): 407-429, 2020.

[10] Shen, X., and Corey, D. R. Chemistry, mechanism and clinical status of antisense oligonucleotides and duplex RNAs. *Nucleic acids research*, *46*(4): 1584-1600, 2018.

[11] Bennett, C. F., and Swayze, E. E. RNA targeting therapeutics: molecular mechanisms of antisense oligonucleotides as a therapeutic platform. *Annual review of pharmacology and toxicology*, *50*: 259-293, 2010.

[12] Crooke, S. T. Molecular mechanisms of antisense oligonucleotides. *Nucleic acid therapeutics*, *27*(2): 70-77, 2017.

[13] Gheibi-Hayat, S. M., and Jamialahmadi, K. Antisense Oligonucleotide (AS-ODN) Technology: Principle, Mechanism and Challenges. *Biotechnology and Applied Biochemistry*, *68*(5): 1086-1094, 2021.

[14] Zamaratski, E., Pradeepkumar, P. I., and Chattopadhyaya, J. A critical survey of the structure-function of the antisense oligo/RNA heteroduplex as substrate for RNase H. *Journal of biochemical and biophysical methods*, *48*(3): 189-208. 2001.

[15] Noy, A., Luque, F. J., and Orozco, M. Theoretical analysis of antisense duplexes: determinants of the RNase H susceptibility. *Journal of the American Chemical Society*, *130*(11): 3486-3496, 2008.

[16] Kiełpiński, Ł. J., Hagedorn, P. H., Lindow, M., and Vinther, J. RNase H sequence preferences influence antisense oligonucleotide efficiency. *Nucleic acids research*, *45*(22): 12932-12944, 2017.

[17] Herbert, C., Dzowo, Y. K., Urban, A., Kiggins, C. N., and Resendiz, M. J. Reactivity and specificity of RNase T1, RNase A, and RNase H toward oligonucleotides of RNA containing 8-Oxo-7, 8-dihydroguanosine. *Biochemistry*, *57*(20): 2971-2983, 2018.

[18] Hagedorn, P. H., Pontoppidan, M., Bisgaard, T. S., Berrera, M., Dieckmann, A., Ebeling, M., ... and Lindow, M. Identifying and avoiding off-target effects of RNase

H-dependent antisense oligonucleotides in mice. *Nucleic Acids Research*, *46*(11): 5366-5380, 2018.

[19] Klumpp, K., Hang, J. Q., Rajendran, S., Yang, Y., Derosier, A., Wong Kai In, P., ... & Martin, J. A. Two-metal ion mechanism of RNA cleavage by HIV RNase H and mechanism-based design of selective HIV RNase H inhibitors. *Nucleic acids research*, *31*(23): 6852-6859, 2003.

[20] Zamecnik, P. C., and Stephenson, M. L. Inhibition of Rous sarcoma virus replication and cell transformation by a specific oligodeoxynucleotide. *Proceedings of the National Academy of Sciences*, *75*(1): 280-284, 1978.

[21] Agrawal, S., Goodchild, J., Civeira, M., Sarin, P. S., and Zamecnik, P. C. Phosphoramidate, phosphorothioate, and methylphosphonateanalogs of oligodeoxynucleotide: inhibitors of replication of human immunodeficiency virus. *Nucleosides & Nucleotides*, *8*(5-6): 819-823, 1989.

[22] Campbell, J. M., Bacon, T. A., and Wickstrom, E. Oligodeoxynucleoside phosphorothioate stability in subcellular extracts, culture media, sera and cerebrospinal fluid. *Journal of biochemical and biophysical methods*, *20*(3): 259-267, 1990.

[23] Zhang, R., Diasio, R. B., Lu, Z., Liu, T., Jiang, Z., Galbraith, W. M., and Agrawal, S. Pharmacokinetics and tissue distribution in rats of an oligodeoxynucleotide phosphorothioate (GEM 91) developed as a therapeutic agent for human immunodeficiency virus type-1. *Biochemical pharmacology*, *49*(7): 929-939, 1995.

[24] Vitravene Study Group. A randomized controlled clinical trial of intravitreousfomivirsen for treatment of newly diagnosed peripheral cytomegalovirus retinitis in patients with AIDS. *American Journal of Ophthalmology*, *133*(4): 467-474, 2002.

[25] Iwamoto, N., Butler, D. C., Svrzikapa, N., Mohapatra, S., Zlatev, I., Sah, D. W., ... and Verdine, G. L. Control of phosphorothioate stereochemistry substantially increases the efficacy of antisense oligonucleotides. *Nature biotechnology*, *35*(9): 845-851, 2017.

[26] Shen, W., De Hoyos, C. L., Migawa, M. T., Vickers, T. A., Sun, H., Low, A., ... and Crooke, S. T. Chemical modification of PS-ASO therapeutics reduces cellular protein-binding and improves the therapeutic index. *Nature biotechnology*, *37*(6): 640-650, 2019.

[27] Geary, R. S., Wancewicz, E., Matson, J., Pearce, M., Siwkowski, A., Swayze, E., and Bennett, F. Effect of dose and plasma concentration on liver uptake and pharmacologic activity of a 2′-methoxyethyl modified chimeric antisense oligonucleotide targeting PTEN. *Biochemical pharmacology*, *78*(3): 284-291. 2009.

[28] Advani, P. P., Paulus, A., Masood, A., Sher, T., and Chanan-Khan, A. Pharmacokinetic evaluation of oblimersen sodium for the treatment of chronic lymphocytic leukemia. *Expert opinion on drug metabolism & toxicology*, *7*(6): 765-774, 2011.

[29] Aartsma-Rus, A. FDA approval of nusinersen for spinal muscular atrophy makes 2016 the year of splice modulating oligonucleotides. *Nucleic acid therapeutics*, *27*(2): 67-69, 2017.

[30] Aartsma-Rus, A., and Krieg, A. M. FDA approves eteplirsen for Duchenne muscular dystrophy: the next chapter in the eteplirsen saga. *Nucleic acid therapeutics*, *27*(1): 1-3, 2017.

[31] Langner, H. K., Jastrzebska, K., and Caruthers, M. H. Synthesis and characterization of thiophosphoramidate morpholino oligonucleotides and chimeras. *Journal of the American Chemical Society*, *142*(38): 16240-16253, 2020.

[32] Nowotny, M., Gaidamakov, S. A., Ghirlando, R., Cerritelli, S. M., Crouch, R. J., and Yang, W. Structure of human RNase H1 complexed with an RNA/DNA hybrid: insight into HIV reverse transcription. *Molecular cell*, *28*(2): 264-276. 2007.

[33] D.A. Case, I.Y. Ben-Shalom, S.R. Brozell, D.S. Cerutti, T.E. Cheatham, III, V.W.D. Cruzeiro, T.A. Darden, R.E. Duke, D. Ghoreishi, M.K. Gilson, H. Gohlke, A.W. Goetz, D. Greene, R Harris, N. Homeyer, Y. Huang, S. Izadi, A. Kovalenko, T. Kurtzman, T.S. Lee, S. LeGrand, P. Li, C. Lin, J. Liu, T. Luchko, R. Luo, D.J. Mermelstein, K.M. Merz, Y. Miao, G. Monard, C. Nguyen, H. Nguyen, I. Omelyan, A. Onufriev, F. Pan, R. Qi, D.R. Roe, A. Roitberg, C. Sagui, S. Schott-Verdugo, J. Shen, C.L. Simmerling, J. Smith, R. SalomonFerrer, J. Swails, R.C. Walker, J. Wang, H. Wei, R.M. Wolf, X. Wu, L. Xiao, D.M. York and P.A. Kollman. AMBER 2018, University of California, San Francisco, 2018.

[34] Frisch, M. J.; Trucks, G.W.; Schlegel, H. B.; Scuseria, G. E.; Robb, M. A.; Cheeseman, J. R.; Scalmani, G.; Barone, V.; Mennucci, B.; Petersson, G. A.; Nakatsuji, H. Gaussian 09, Revision D. 01, Gaussian, Inc., Wallingford CT, 2009.

[35] Wang, Y., Verma, P., Jin, X., Truhlar, D. G., and He, X. Revised M06 density functional for main-group and transition-metal chemistry. *Proceedings of the National Academy of Sciences*, *115*(41): 10257-10262, 2018.

[36] Jorgensen, W. L., Chandrasekhar, J., Madura, J. D., Impey, R. W., and Klein, M. L. Comparison of simple potential functions for simulating liquid water. *The Journal of chemical physics*, *79*(2): 926-935,1983.

[37] Machireddy, B., Kalra, G., Jonnalagadda, S., Ramanujachary, K., and Wu, C. Probing the binding pathway of BRACO19 to a parallel-stranded human telomeric G-quadruplex using molecular dynamics binding simulation with AMBER DNA OL15 and ligand GAFF2 force fields. *Journal of chemical information and modeling*, *57*(11): 2846-2864, 2017.

[38] Zhao, J., Kennedy, S. D., and Turner, D. H. Nuclear magnetic resonance spectra and AMBER OL3 and ROC-RNA simulations of UCUCGU reveal force field strengths and weaknesses for single-stranded RNA. *Journal of Chemical Theory and Computation*, *18*(2): 1241-1254, 2022.

[39] Cheatham, T. I., Miller, J. L., Fox, T., Darden, T. A., and Kollman, P. A. Molecular dynamics simulations on solvated biomolecular systems: the particle mesh Ewald method leads to stable trajectories of DNA, RNA, and proteins. *Journal of the American Chemical Society*, *117*(14): 4193-4194, 1995.

[40] Miyamoto, S., & Kollman, P. A. Settle: An analytical version of the SHAKE and RATTLE algorithm for rigid water models. *Journal of computational chemistry*, *13*(8): 952-962, 1992.

[41] Roe, D. R., and Cheatham III, T. E. PTRAJ and CPPTRAJ: software for processing and analysis of molecular dynamics trajectory data. *Journal of chemical theory and computation*, *9*(7): 3084-3095, 2013.

[42] Xu, L., Sun, H., Li, Y., Wang, J., and Hou, T. Assessing the performance of MM/PBSA and MM/GBSA methods. 3. The impact of force fields and ligand charge models. *The journal of physical chemistry B*, *117*(28): 8408-8421, 2013.

[43] Ho, P. S., and Carter, M. DNA structure: alphabet soup for the cellular soul. In *DNA replication-current advances*. IntechOpen, 2011.

[44] Xia, Z., Bell, D. R., Shi, Y., and Ren, P. RNA 3D structure prediction by using a coarse-grained model and experimental data. *The Journal of Physical Chemistry B*, *117*(11): 3135-3144, 2013.

[45] Hanessian, S., Schroeder, B. R., Giacometti, R. D., Merner, B. L., Østergaard, M., Swayze, E. E., and Seth, P. P. Structure-Based Design of a Highly Constrained Nucleic Acid Analogue: Improved Duplex Stabilization by Restricting Sugar Pucker and Torsion Angle γ. *AngewandteChemie International Edition*, *51*(45): 11242-11245, 2012.

[46] Heinemann, U., and Roske, Y. Symmetry in nucleic-acid double helices. *Symmetry*, *12*(5): 737, 2020.

[47] Parker, T. M., Hohenstein, E. G., Parrish, R. M., Hud, N. V., and Sherrill, C. D. Quantum-mechanical analysis of the energetic contributions to π stacking in nucleic acids versus rise, twist, and slide. *Journal of American Chemical Society*, 135(4):1306-1316, 2013.

[48] Chen, F., Sun, H., Wang, J., Zhu, F., Liu, H., Wang, Z., ... and Hou, T. Assessing the performance of MM/PBSA and MM/GBSA methods. 8. Predicting binding free energies and poses of protein–RNA complexes. *Rna*, *24*(9): 1183-1194, 2018.

[49] Yakovchuk, P., Protozanova, E., and Frank-Kamenetskii, M. D. Base-stacking and base-pairing contributions into thermal stability of the DNA double helix. *Nucleic acids research*, *34*(2): 564-574, 2006.

[50] Sponer, J., Zgarbová, M., Jurecka, P., Riley, K. E., Sponer, J. E., and Hobza, P. Reference quantum chemical calculations on RNA base pairs directly involving the 2′-OH group of ribose. *Journal of Chemical Theory and Computation*, *5*(4): 1166-1179, 2009.

[51] Butcher, S. E., and Pyle, A. M. The molecular interactions that stabilize RNA tertiary structure: RNA motifs, patterns, and networks. *Accounts of chemical research*, *44*(12): 1302-1311, 2011.